1-1-2007

Performance enhancement techniques for variable spreading factor OFCDM systems

Lamiaa Khalid
Ryerson University

PERFORMANCE ENHANCEMENT TECHNIQUES FOR VARIABLE SPREADING FACTOR OFCDM SYSTEMS

by

Lamiaa Khalid

B.Sc., Ain Shams University, Cairo, Egypt, 2000

A Thesis

Presented to the School of Graduate Studies at

Ryerson University

in partial fulfilment of the

requirements for the degree of

Master of Applied Science

in the Program of Electrical and Computer Engineering

Toronto, Ontario, Canada, December 2007

Abstract

Performance Enhancement Techniques for Variable Spreading Factor OFCDM Systems

Master of Applied Science
Electrical and Computer Engineering
Ryerson University

In this thesis, we investigate the effect of Carrier Frequency Offset (CFO) on the performance of downlink Variable Spreading Factor (VSF) OFCDM systems when subcarrier grouping is used. An analytic expression of the SINR is derived for downlink VSF-OFCDM with CFO for the case of maximal ratio combining receiver. Numerical results show that, when the total spreading factor is fixed, the VSF-OFCDM system with higher frequency domain spreading factor is more sensitive to CFO than that with lower frequency domain spreading factor. Due to the adverse impact of the CFO on VSF-OFCDM systems, we propose a correction scheme based on the maximum likelihood principle. We derive the likelihood function for VSF-OFCDM system with CFO and use a gradient algorithm to estimate and minimize the effect of CFO in a tracking mode. Our results show that the BER performance in the low SNR environment can be improved significantly with few number of iterations for different spreading factors. We also propose a threshold-based group-adaptive modulation algorithm used with an adaptive subcarrier allocation technique for downlink VSF-OFCDM to increase the spectral efficiency for a given target BER. The proposed algorithm provides an increase in spectral efficiency without increasing the total transmit power for different spreading factors with and without coding.

Acknowledgement

I would like to express my sincere gratitude to my supervisor, Prof. Alagan Anpalagan for his continuous encouragement and support. He was always generous with his invaluable time and always motivating me and teaching me by example how to become competent and professional. It was a great privilege to work with him.

I would like to acknowledge the Department of Electrical and Computer Engineering and the School of Graduate Studies at Ryerson University for their support in terms of financial aid, and work experience as a graduate assistant.

I would also like to thank my defense committee for taking the time and effort to review my work and provide me with their insightful comments.

Thanks are also due to my colleagues in the WAN group present and past, I am lucky to be a part of this group where a team spirit truly prevails. I would especially like to thank Ryan Caldwell for his help in the early stages of this work.

I can never find the words to thank my husband, Osama Bazan, who was amazingly patient and understanding and who helped me through the most difficult times of my life. He not only believed in me and was always supportive but he also offered me his advice and his valuable help whenever I needed it.

My special thanks goes to my parents, especially my mother who is always a great source of love and motivation, I could never thank her enough for everything she has done for me. I would also like to thank my parents in-law and my siblings for their love and encouragement.

My deepest love and gratitude is to my grandmother, if it were not for her, I would not be where I am today. Thank you for all the little and great things you have done for me, you will forever live in my heart. Last but not least, I would like to thank my son, Zeyad, who is my constant source of joy and who always gives me a reason to smile.

Contents

List of Figures

List of Tables

List of Abbreviations

4G	Fourth Generation
AWGN	Additive White Gaussian Noise
B3G	Beyond Third Generation
BER	Bit Error Rate
CDMA	Code Division Multiple Access
BPSK	Binary Phase Shift Keying
CFO	Carrier Frequency Offset
CP	Cyclic Prefix
DFT	Discrete Fourier Transform
FDMA	Frequency Division Multiple Access
FEC	Forward Error Correction
FFT	Fast Fourier Transform
ICI	Intercarrier Interference
IFFT	Inverse Fast Fourier Transform
i.i.d	independent identically distributed
IP	Internet Protocol
ISI	Intersymbol Interference
MAI	Multiple Access Interference
MC-CDMA	Multicarrier CDMA
MC-DS-CDMA	Multicarrier Direct Sequence CDMA
ML	Maximum Likelihood
MRC	Maximal Ratio Combining
OFCDM	Orthogonal Frequency And Code Division Multiplexing
OFDM	Orthogonal Frequency Division Multiplexing
PN	Pseudo-Noise

P/S	Parallel-to-Serial
PSK	Phase Shift Keying
QAM	Quadrature Amplitude Modulation
QPSK	Quadrature Phase Shift Keying
SF	Spreading Factor
SINR	Signal to Interference and Noise Ratio
SNR	Signal to Noise Ratio
S/P	Serial-to-Parallel
TDMA	Time Division Multiple Access
VSF	Variable Spreading Factor

Chapter 1

Introduction

The Fourth Generation (4G) of wireless communications systems, also known as Beyond Third Generation (B3G) systems, have sparked much interest in the recent years. Among the foreseen future applications the 4G system is predicted to bring to users are high streaming video, multimedia and internet access. Higher data rates, an increase of capacity in the radio link and seamless mobility across heterogeneous access networks are some of the most recognized traits for 4G [1]. Many believe that one of the strongest aspects of 4G involves the merger of cellular and wireless technologies rather than being an entirely new standard [2]. The most agreed upon traits for 4G by researchers is that the air link will be packet-switched under the Internet Protocol (IP) [3]. To achieve the performance required of the 4G systems, new technologies related to multiple access, adaptive modulation and coding must be developed to be used in conjunction with the previous technologies.

4G systems are likely to employ improved multiple access schemes to achieve the expected throughput of 100Mbps and 20Mbps in the downlink and uplink of a cellular system, respectively [3]. 4G is expected to rely heavily on Orthogonal Frequency Division Multiplexing (OFDM) based techniques [4]. OFDM is currently used in some of the wireless network standards such as 802.11a, 802.11g and 802.16 (WiMAX) to provide high data rates. OFDM uses parallel transmission of data symbols on orthogonal subcarriers to reduce the trans-

mission rate and increase the symbol duration thus enabling data transmission with very low Intersymbol Interference (ISI). Some variations of OFDM which allow multiple access are Multicarrier Direct Sequence CDMA (MC-DS-CDMA) [5], Multicarrier CDMA (MC-CDMA) [6, 7] and Orthogonal Frequency and Code Division Multiplexing (OFCDM) [8]. In MC-DS-CDMA the data symbols are serial-to-parallel converted and spread using a spreading sequence in the time domain which provides flexible data rates and reduces the Multiple Access Interference (MAI). MC-CDMA is essentially an OFDM technique where the individual data symbols are spread using a spreading code in the frequency domain. The main advantage of MC-CDMA is the frequency diversity gained by transmitting over subcarriers experiencing independent fading.

OFCDM which is based on MC-CDMA, is being studied as the most recent candidate for 4G. In OFCDM, data streams are segmented into multiple substreams and spread over successive symbols in the time domain and over successive subcarriers in the frequency domain, thus combining time and frequency domain spreading. The main advantage of OFCDM is the diversity gained as symbols are replicated in time and across several frequency subcarriers. The Variable Spreading Factor (VSF) OFCDM, which changes the Spreading Factor (SF) in both the time and frequency domain, was proposed in [9–11]. NTT-DoCoMo, a major Japanese mobile provider, had successfully conducted a 100Mbps downlink and 20Mbps uplink experiment in an indoor environment, using experimental 4G mobile communications system employing the VSF-OFCDM technologies [3]. In OFCDM, the total spreading factor SF, is expressed as $SF = SF_{time} \times SF_{freq}$, where SF_{time} and SF_{freq} represent the spreading factors in the time and frequency domain respectively. By employing the VSF in OFCDM, the appropriate SF_{time} and SF_{freq} can be adaptively changed according to the cell structure, channel load and radio link conditions such as delay spread.

Introducing VSF-OFCDM as a likely candidate for 4G sparks much research in this technology with the aim of improving the overall performance of the 4G systems and overcoming any potential problems. One of the methods of improving the performance of multicarrier

systems is to use adaptive subcarrier allocation techniques which were proven to outperform the respective non-adaptive systems in terms of the Bit Error Rate (BER) performance [12, 13]. An adaptive subcarrier allocation technique was proposed in [14] for the OFCDM system. It was shown that, using adaptive subcarrier allocation in OFCDM improves the mean BER performance when compared to the respective non-adaptive OFCDM system.

One of the main drawbacks of multicarrier systems is the problem of Carrier Frequency Offset (CFO) which severely degrades their performance [15–17], and VSF-OFCDM systems are no exception. There are two main adverse effects caused by carrier frequency offset. The first is the reduction of the desired signal amplitude since the signals are no longer sampled at their peaks and the second is the generation of Intercarrier Interference (ICI) resulting in interchip interference between and within codes [18]. In this thesis, we enhance the performance of a VSF-OFCDM system with adaptive subcarrier allocation through providing a detailed analysis of the effect of CFO on VSF-OFCDM systems using BPSK modulation and investigating the different types of ICI and the expected performance degradation. We then propose a compensation technique in the tracking mode based on the Maximum Likelihood (ML) estimation principle [19, 20].

The demand for high data rates in future wireless communications has made it essential to investigate methods of achieving high spectral efficiency since the spectrum is considered a valuable commodity. Adaptive modulation proposed by Hanzo and Torrance [21] can help maximize the data rates over wireless channels. This is accomplished by adapting the modulation levels to the changing channel conditions and thus making use of spectrally efficient modulation schemes. In this thesis, we aim to improve the spectral efficiency of the VSF-OFCDM system by an adaptive modulation algorithm that is performed on groups of subcarriers to maintain the BER below a certain performance threshold. This algorithm switches the modulation level between BPSK, QPSK, 8PSK and 16QAM depending on the estimated Signal to Interference and Noise Ratio (SINR) for each group.

1.1 Thesis Contributions

The key contributions of this thesis can be summarized in the following points:

- We analyze in details the types and amount of interference caused by the carrier frequency offset in VSF-OFCDM when subcarrier grouping is used [22].
- We derive a closed form expression for the total SINR for a VSF-OFCDM system in the presence of the different types of interference. To the best of our knowledge, this is the first detailed analysis for VSF-OFCDM with carrier frequency offset [22].
- We evaluate the BER performance degradation under various carrier frequency offsets for different time and frequency spreading factors [22].
- We propose a carrier frequency offset correction scheme for VSF-OFCDM in a tracking mode based on the maximum likelihood estimation principle [23].
- We evaluate the BER performance enhancement with the proposed correction scheme for different spreading factors [23].
- We propose a threshold-based group-adaptive modulation algorithm for VSF-OFCDM systems to increase the spectral efficiency for a predefined target BER [24].
- We evaluate the performance of our adaptive modulation algorithm in terms of the spectral efficiency of the VSF-OFCDM system with and without coding to meet different target BER requirements [25].
- We assess the improvement in spectral efficiency of the VSF-OFCDM system when adaptive subcarrier allocation is employed [25].

1.2 Thesis Organization

This thesis is organized as follows

In chapter 2, the advantages of multicarrier modulation and the description of the OFDM system and its variations are presented. This includes a description of MC-DS-CDMA systems, MC-CDMA systems and the two dimensionally spread OFCDM system.

In chapter 3, we outline in details the system model used in this study. We discuss the subcarrier grouping strategy that is used in our work. We also provide the system model for the VSF-OFCDM system. This includes a description of the transmitter and receiver, the adaptive subcarrier allocation scheme used, as well as the channel model.

In chapter 4, we investigate the effect of Carrier Frequency Offset (CFO) on the performance of downlink VSF-OFCDM systems and propose a scheme for its correction. We analyze the BER of VSF-OFCDM taking into account the effect of frequency offset when subcarrier grouping is used. We present the results in terms of the performance degradation in BER due to CFO. Following this, we propose a CFO correction scheme based on the maximum likelihood estimation principle. After deriving the likelihood function for the VSF-OFCDM system with CFO, we use a gradient algorithm to estimate and minimize the effect of CFO in a tracking mode. The results of using this CFO correction scheme are also presented in this chapter.

In chapter 5, we propose an adaptive modulation algorithm for the VSF-OFCDM system that is performed on groups of subcarriers to increase the spectral efficiency without sacrificing the BER performance under different spreading factors assuming there is no CFO. We use a fixed threshold to switch between modulation levels depending on the estimated SINR of the users in each group. We use coding to decrease the required SINR to achieve a target BER. The performance improvement in terms of spectral efficiency is presented for different spreading factors and the results are compared with the non-adaptive OFCDM system. We also compare the spectral efficiency of the VSF-OFCDM system using adaptive modulation with and without adaptive subcarrier allocation.

In chapter 6, we conclude the thesis with a highlight on the important results and their interpretation. Also, possible future work is presented in this chapter.

Chapter 2

OFDM and Multicarrier CDMA

Traditional single carrier modulation techniques give good data rates but their performance is limited when used in fading channels. Any attempt to mitigate the multipath effects results in an increased system complexity. The idea of multicarrier transmission has surfaced recently to be used for combating the hostility of wireless channel. Improved performance in bad channel conditions, high data rates and efficient use of the bandwidth are the primary advantages of multicarrier modulation.

In the following sections, we discuss the advantages of using multicarrier techniques and Orthogonal Frequency Division Multiplexing (OFDM). A description of various multicarrier CDMA systems is also discussed. This includes MC-DS-CDMA, MC-CDMA and a description of OFCDM, which is the focus of this thesis.

2.1 Advantages of Multicarrier Modulation

Mobile radio channels introduce severe multipath propagation due to multiple scattering from objects in the vicinity of the mobile unit. This scattering introduces rapid fluctuation of the received signal envelope as well as phase variations. The envelope of the received signal is typically Rayleigh distributed. Also the motion of the mobile unit introduces a Doppler shift which causes a broadening of the signal spectrum [26]. The multipath channel can

also be frequency selective where the fading envelope of the received signal at one frequency might not be correlated with the envelope at another frequency. This is due to the fact that the symbol duration might be less than the maximum delay spread. As a result, the received signal consists of overlapping versions of the transmitted symbols resulting in ISI.

In a conventional serial data transmission, the symbols are transmitted sequentially with the frequency spectrum of each transmitted symbol occupying the entire bandwidth available. The delay spread of the channel dictates the symbol duration or alternatively the data rate that can be achieved to prevent the effects of the ISI. The idea behind multicarrier transmission is to split the data stream into substreams of lower data rates and transmit these data substreams on adjacent subcarriers, this can be regarded as a parallel transmission in the frequency domain, and it does not affect the total bandwidth that is needed. The main advantage of this approach is that the parallel transmission increases the symbol time by modulating the symbols into narrow subchannels which makes them more robust to the channel delay spread effects and therefore, allows for a higher data rate for a given delay spread [27].

2.2 OFDM

OFDM is a special form of multicarrier transmission. In OFDM, the available bandwidth is split into several narrow bands and data can be modulated into different subcarriers centered at these bands. The use of parallel transmission effectively increases the symbol duration and considerably reduces ISI [27]. By choosing the subcarrier bandwidth to be less than the coherence bandwidth of the channel, they experience almost flat fading which makes equalization very simple. The subcarriers used in OFDM systems are orthogonal, to ensure proper retrieval of data at the receiver end and to minimize interference. The orthogonality of the subcarriers allows the spectra of individual subcarriers to overlap each other without any significant interference which allows for more efficient use of the bandwidth. Also, OFDM

is very robust to narrow band interference because such interference can only affect a small percentage of the subcarriers.

The subcarriers are separated by a frequency of $1/T_s$, where T_s is the symbol duration to ensure that the subcarriers are orthogonal over a symbol duration (in the absence of channel distortion). If the channel is slowly time varying, the capacity can be enhanced significantly by adapting the data rate per subcarrier according to the Signal to Noise Ratio (SNR) of that subcarrier [28].

The main difficulty in using the parallel data system is the complexity of the equipment needed for the implementation of the system. This is because OFDM requires very accurate frequency synchronization between the receiver and the transmitter; with frequency deviation, the subcarriers will no longer be orthogonal, causing Intercarrier Interference (ICI) which will reduce the system performance [21]. The employment of the Discrete Fourier Transform (DFT) to replace the banks of sinusoidal generators and the demodulators was suggested by Weinstein and Ebert in [29], which significantly reduces the implementation complexity of OFDM modems. This operation is equivalent to multiplying each bit by the desired subcarrier frequency; however, it ensures exact frequency spacing and phase coherence between subcarriers. The discrete Fourier transform can in turn be implemented using a Fast Fourier Transform (FFT) algorithm particularly when the number of subcarriers is large. The total number of subcarriers translates into the number of points of the FFT. Fig. 2.1 shows a simplified implementation of OFDM using FFT engines.

Cyclic Prefix

Cyclic prefix is a crucial feature of OFDM which is used to combat the ISI introduced by the multipath channel through which the signal is propagated. The basic idea is to replicate part of the OFDM time domain waveform from the back to the front to create a guard period. The duration of the guard period T_g should be longer than the maximum delay spread of the channel. Fig. 2.2 shows the cyclic prefix format. At the receiver, certain position within

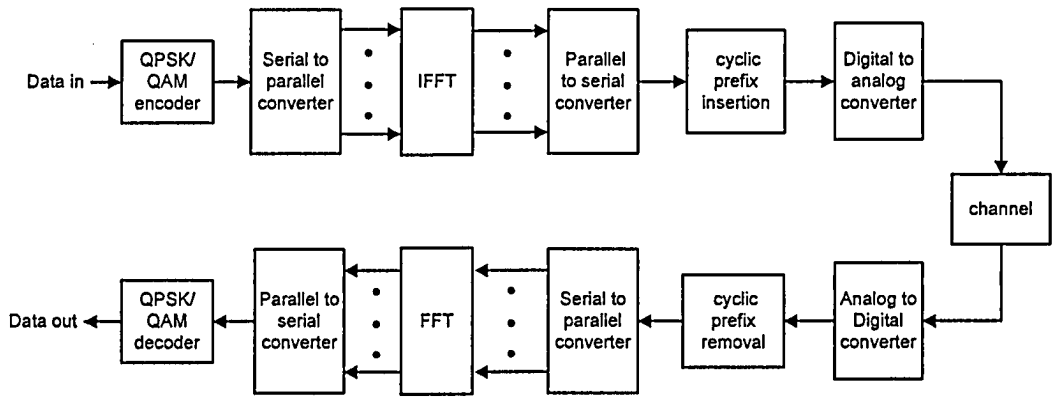

Figure 2.1: Block diagram of OFDM system.

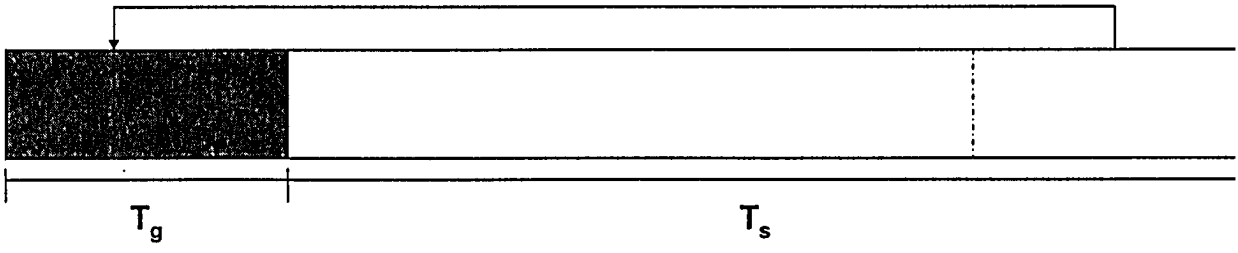

Figure 2.2: Cyclic prefix format.

the cyclic prefix (T_x) is chosen as the sampling starting point, which satisfies the criteria

$$\tau_{max} < T_x < T_g, \tag{2.1}$$

where τ_{max} is the maximum delay spread of the channel. Once the above condition is satisfied, there is no ISI since the previous symbol will only have effect over samples within $[0, \tau_{max}]$. Since sampling starts after τ_{max}, there is no ISI. The cyclic prefix also aids in synchronization at the receiver because it can be used to identify the beginning of an OFDM symbol.

2.3 Multicarrier CDMA

Code Division Multiple Access (CDMA) is considered a strong candidate to support multimedia mobile services because it has the ability to cope up with the asynchronous nature of the multimedia traffic and can provide higher capacity as opposed to the conventional access schemes such as Time Division Multiple Access (TDMA) or Frequency Division Multiple Access (FDMA). By employing Rake receivers, CDMA systems can coherently combine the multipath components due to the hostile frequency selective channel. The processing gain due to spreading provides robustness to the multiuser interference. The use of conventional CDMA does not seem to be realistic when the data rates become very high due to severe ISI and the difficulty in synchronizing a fast sequence. Techniques for reducing the symbol and chip rate are essential in this case.

Combining multicarrier OFDM transmissions with CDMA spreading allows us to use the available spectrum in an efficient way and retain the many advantages of a CDMA system [6]. The use of multicarrier CDMA not only mitigates the effect of ISI but also exploits the multipath effect. In [30], it was shown that multicarrier CDMA suffers slightly in the presence of interference as opposed to DS-CDMA whose performance decreases significantly in the presence of interference. Hence, this combination of OFDM-CDMA is a useful technique for 4G systems where variable data rates are needed as well as reliable communication systems. Prasad and Hara [31] compared various methods of combining the two techniques, based on spreading operation that takes place either in time or frequency domain. The OFDM with spreading in time or frequency domain only is known as Multicarrier DS-CDMA (MC-DS-CDMA) and Multicarrier CDMA (MC-CDMA), respectively. The multicarrier system with two dimensional spreading was proposed in [8,32], where spreading is employed in both time and frequency domains simultaneously. This is known as Orthogonal Frequency and Code Division Multiplexing (OFCDM). Fig. 2.3 illustrates time domain, frequency domain, and two dimensional spreading schemes respectively in multicarrier systems. It can be seen that instead of placing the spread chips in only time or frequency domain, the 2-D spreading

locates the chips in blocks on the time-frequency grid. Basically, frequency domain spreading introduces frequency diversity, whereas time domain spreading mainly provides flexibility of different data rates.

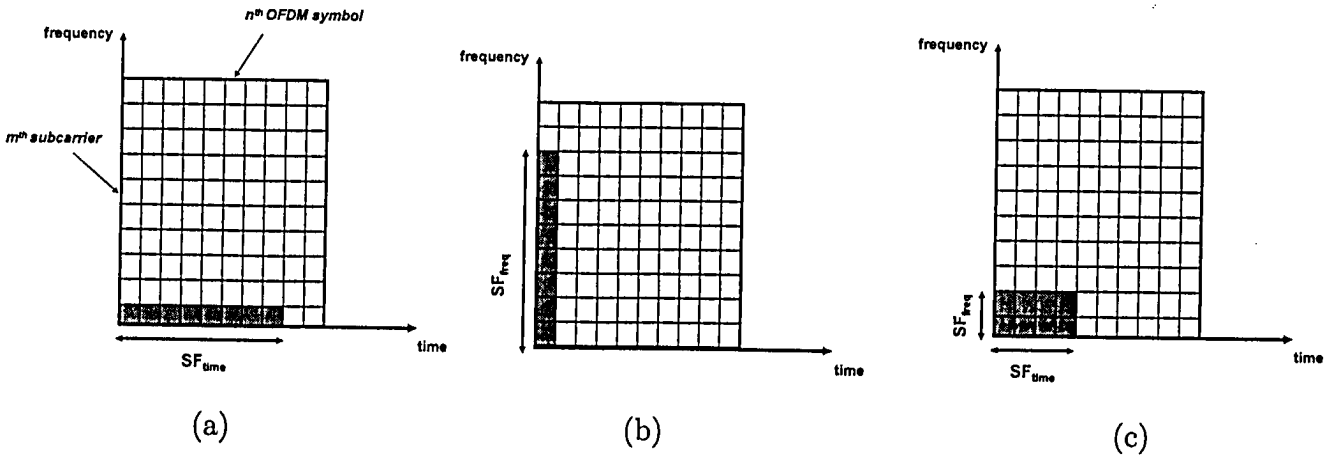

Figure 2.3: Different spreading schemes in multicarrier systems: (a) spreading in time domain (MC-DS-CDMA) (8x1) (b) spreading in frequency domain (MC-CDMA) (1x8) (c) 2-D spreading (OFCDM) (4x2).

Spreading

Spreading the information symbols to be transmitted with the aid of orthogonal codes is the basis of supporting multiple access capabilities of multicarrier CDMA systems [7]. Instead of transmitting each complex symbol delivered by the modulator separately on a specific subcarrier as in the OFDM modems, its influence is spread over several subcarriers with the aid of orthogonal multichip spreading codes. The advantage of employing orthogonal codes for performing the spreading is related to the resultant simple receiver design. A prominent class of orthogonal codes, which are often used in CDMA systems is constituted by the family of orthogonal Walsh codes. The operation of spreading with the aid of these codes can be implemented in form of a fast transform, which takes advantage of the recursive structure of the codes, similar to the FFT [21].

Walsh-Hadamard sequences are bipolar spreading sequences that are used for channel

separation in DS-CDMA. They are orthogonal sequences with zero cross correlation in ideal conditions and are easy to generate. However, the correlation between sequences can increase due to delays or shifts between them due to practical conditions. The Walsh-Hadamard sequences of length N where $N = 2^n$; $n = 1, 2, \cdots$, are often defined recursively using Hadamard matrices H_N, with

$$H_2 = \frac{1}{\sqrt{2}} \begin{pmatrix} +1 & +1 \\ +1 & -1 \end{pmatrix}, \tag{2.2}$$

and,

$$H_{2N} = \frac{1}{\sqrt{2}} \begin{pmatrix} H_N & H_N \\ H_N & -H_N \end{pmatrix}. \tag{2.3}$$

Some of the important properties of the Walsh code include

- Zero cross correlation between the codes,
- The scaled inner product of each code is 1,
- The number of 1's and -1's are equal in each code sequence.

For the despreading operation, since the Walsh code of the user is not known at the receiver, a search operation is done where the received symbols are correlated to the Walsh codes and the codes with maximum correlation with the received symbols are chosen. Due to their very regular structure, Walsh-Hadamard sequences are characterized with very poor auto-correlation properties. In real systems, this is alleviated by the use of scrambling codes on the top of Walsh-Hadamard sequences. These are normally very long codes having very distinctive peaks at zero in their auto-correlation functions. In addition to improving synchronization properties, scrambling also helps in reducing Multiple Access Interference (MAI).

2.3.1 MC-DS-CDMA

The MC-DS-CDMA system spreads the serial-to-parallel converted input data stream using the CDMA spreading code, which corresponds to spreading in the time domain, and then modulates a different subcarrier with each of the spread data streams. The subcarriers are orthogonal to each other with minimum frequency separation [5]. MC-DS-CDMA can provide a performance improvement over DS-CDMA systems that operate in wideband channels, because the narrowband subchannels are resistant to ISI. They are also very effective in providing multiple access with very low MAI. This occurs because the coherence time of the channel is generally much larger than the duration of the transmitted symbol which allows the Pseudo-Noise (PN) codes to retain orthogonality. The main drawback of MC-DS-CDMA is that fading may corrupt the transmission since only one subcarrier is used during each transmission interval. The transmitter block for MC-DS-CDMA is shown in Fig. 2.4 for user k, where G_{MD} denotes the processing gain, and the spreading code for user k is given by $c^{T(k)} = [c_1^{T(k)}, c_2^{T(k)}, \cdots, c_{G_{MD}}^{T(k)}]$ and each chip belongs to the set $\{1, -1\}$. The receiver block is shown in Fig. 2.5 where the despreading is done in the time domain after the FFT followed by low pass filtering and demodulation. The figures are adopted from [31].

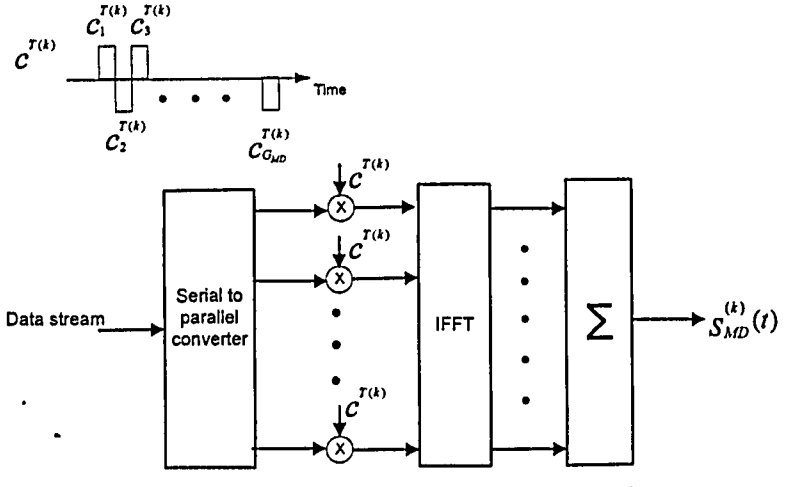

Figure 2.4: MC-DS-CDMA transmitter.

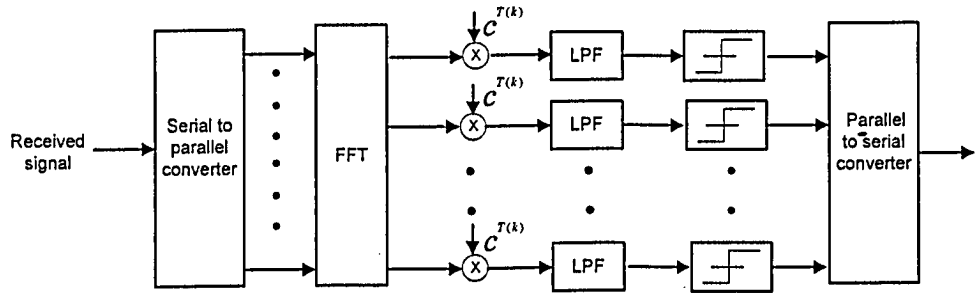

Figure 2.5: MC-DS-CDMA receiver.

2.3.2 MC-CDMA

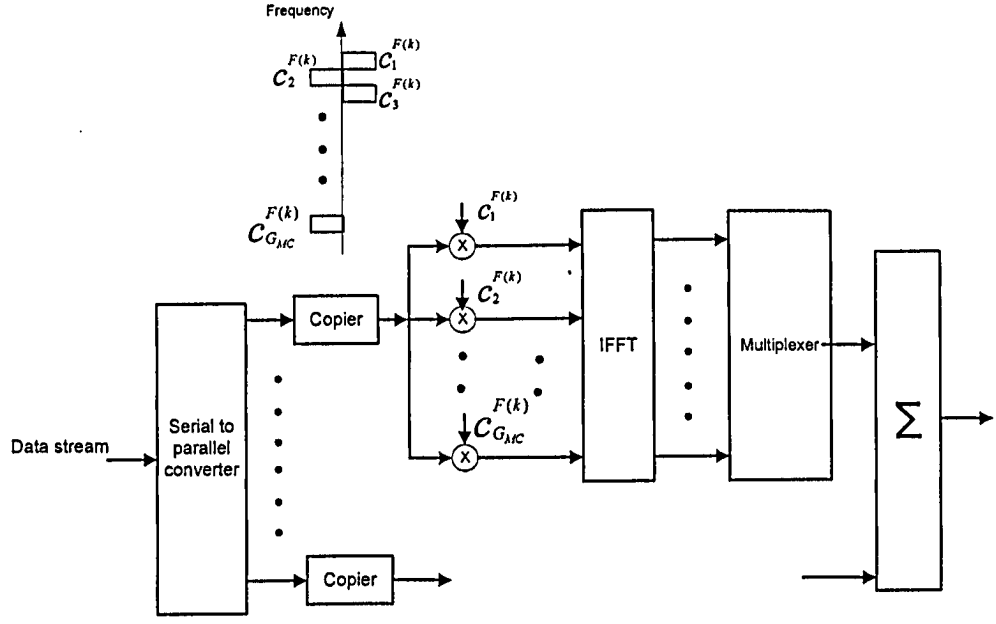

Figure 2.6: MC-CDMA transmitter.

MC-CDMA implements frequency domain spreading via orthogonal codes; thus, several users transmit over the same subcarrier. In MC-CDMA, a fraction of the symbol corresponding to a chip of the frequency domain spreading code is transmitted through a different subcarrier [6, 33].

In [31], it was shown that MC-CDMA outperforms MC-DS-CDMA in terms of downlink

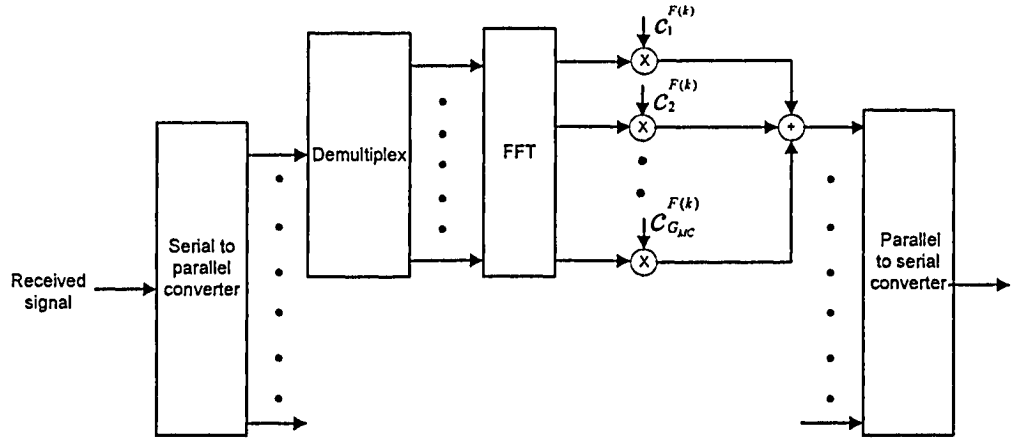

Figure 2.7: MC-CDMA receiver.

BER performance. The reason is that the MC-CDMA scheme can always use all the received signal scattered in frequency domain compared to the MC-DS-CDMA scheme thus providing frequency diversity although it requires a much complex receiver.

The main drawback of MC-CDMA systems is that an excessive amount of multiple access interference may be experienced when transmitting through a frequency selective channel. This occurs because the PN sequences lose orthogonality if the amplitude level of the PN chips is altered during the symbol period. Since each subcarrier experiences independent fading, and each subcarrier is multiplied by one chip from the PN sequence, a loss of orthogonality is common. As a result, the performance of MC-CDMA systems degrades with high channel loads due to the excessive MAI [10].

The transmitter block for MC-CDMA is shown in Fig. 2.6, where G_{MC} denotes the processing gain and the spreading code for user k is given by $c^{F(k)} = [c_1^{F(k)}, c_2^{F(k)}, \cdots, c_{G_{MC}}^{F(k)}]$. The data stream is first serial-to-parallel converted into parallel sequences because it is crucial for multicarrier transmission to have frequency non-selective fading over each subcarrier [31], then, the data is spread over the frequency domain, where each sequence is mapped onto G_{MC} subcarriers. An exact inverse of the transmitter is performed at the receiving end. The FFT is performed to demodulate the signals followed by the despreading as shown in Fig.

2.7. The figures are adopted from [31].

2.3.3 OFCDM

In OFCDM, data streams are segmented into multiple substreams and spread by the spreading sequence, which is the combination of an orthogonal short channelization code and the cell-specific long scrambling code using short Walsh-Hadamard codes and long PN codes. Each chip of the resultant sequence is allocated to the successive OFCDM symbols in the time domain (called time domain spreading) and to the successive subcarriers in the frequency domain (called frequency domain spreading). The Variable Spreading Factor (VSF) OFCDM, which changes the Spreading Factor (SF) in both the time and frequency domain, was proposed in [9]. The total spreading factor SF, is expressed as $SF = SF_{time} \times SF_{freq}$, where SF_{time} and SF_{freq} represent the spreading factors in the time and frequency domain respectively. In VSF-OFCDM, although the data rate is reduced by $1/SF$ due to replication, compared to the non-spreading cases like OFDM, the total data rate is increased by introducing the code multiplexing of different users with different orthogonal short channelization codes.

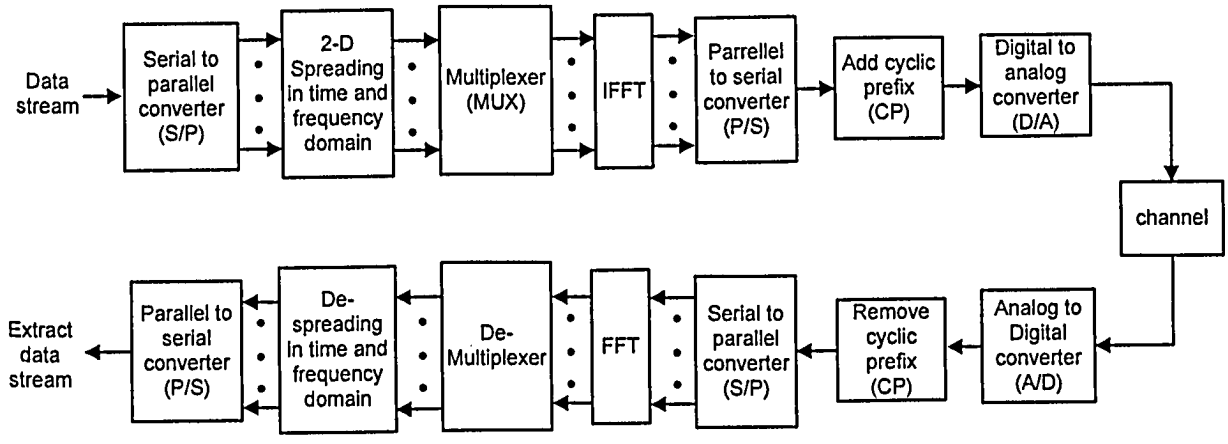

Figure 2.8: OFCDM block diagram.

The modulation and demodulation of OFCDM are almost identical to those in OFDM.

The difference lies in data spreading by means of spreading codes. A block diagram for the FFT based OFCDM system is shown in Fig. 2.8. At the transmitter, the data streams are serial-to-parallel converted and then fed into different subcarriers, applying code spreading and Inverse Fast Fourier Transform (IFFT) to generate OFCDM signals. After IFFT, the signals undergo parallel-to-serial conversion and Cyclic Prefix (CP) addition. At the receiver, the CP is first removed and then each subcarrier corresponding to the received signal is coherently detected with FFT, followed by code despreading. After that, parallel-to-serial conversion is performed, and the data is recovered.

Since OFCDM employs time and frequency domain spreading simultaneously, it experiences the favorable qualities of both MC-CDMA and MC-DS-CDMA systems discussed in the previous sections. The use of frequency domain spreading allows the system to benefit from frequency diversity, while time domain spreading allows for flexible data rates and multiple access with low interference. As a result of these benefits, OFCDM has been shown to provide more favorable BER performance than MC-CDMA and MC-DS-CDMA systems [8,34].

Since the overall received signal quality employing two dimensional spreading through a multipath fading channel depends on the tradeoff relationship between the increasing frequency diversity effect and the impairment of code orthogonality, there are particular time and frequency domain spreading factors that are the most favorable under various conditions. As a result, in VSF-OFCDM, the parameters SF_{time} and SF_{freq} are adaptively controlled as per the cell structure, the channel load and the radio link conditions.

For a fixed SF, the authors in [10,11] propose to prioritize the time domain spreading. The reason is that within a frame duration, which is typically in the order of 0.5-1.0 msec, channel variation in the time domain is slight whereas the channel variation in the frequency domain increases due to frequency selective fading. Also, time domain spreading leads to lower intercode interference level. Frequency domain spreading is applied mainly for low data rate and low channel loads in order to gain frequency diversity gains.

In the next chapter, we will discuss in details the system model for the VSF-OFCDM system used in our work as well as the rationale behind some of the assumptions made in our analysis.

Chapter 3

VSF-OFCDM System Model

In this chapter, we outline in details the system model used in this study. First, we discuss the subcarrier grouping strategy that is used to maximize the frequency diversity and minimize MAI. Following this, we provide the system model for the VSF-OFCDM system. This includes a description of the transmitter and receiver, the adaptive subcarrier allocation scheme used in our work, as well as the channel model used in the analysis and the Monte Carlo simulations.

3.1 Subcarrier Grouping

In [14], the authors proposed the use of subcarrier grouping to improve the performance of the OFCDM system. Using this strategy, the total number of subcarriers M_c is divided into several small, non-contiguous groups. In particular, the total spectrum is divided into G groups; each group g has M non-contiguous subcarriers that are equally spaced throughout the spectrum, where, the spectral separation of the subcarriers in the same group is identical to the total number of groups. Fig 3.1 shows an example of the subcarrier grouping strategy, with three subcarrier groups.

Since the subcarriers in each group are separated equally throughout the bandwidth, the frequency spacing is likely to be larger than the coherence bandwidth of the channel. This

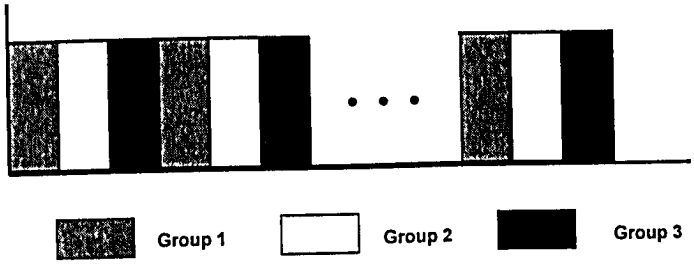

Figure 3.1: Subcarrier grouping with 3 subcarriers groups.

ensures that the fading on all subcarriers in the same group is uncorrelated, allowing the system to achieve the maximum benefit from frequency diversity. Also, since the number of subcarriers in each group is small, the amount of MAI caused by frequency domain spreading is minimized [14].

3.2 VSF-OFCDM System Model

3.2.1 VSF-OFCDM Transmitter

An OFCDM system with K simultaneous users is considered. The total spectrum (M_c subcarriers) is divided into G groups; each group has M non-contiguous subcarriers that are equally spaced throughout the spectrum. A block diagram of the VSF-OFCDM transmitter is shown in Fig. 3.2. Each data symbol in the OFCDM system is spread in the time domain with N chips, where N is equal to SF_{time}, and in the frequency domain with SF_{freq} chips which are equal to the M subcarriers in each group g. Therefore, totally $SF = SF_{time} \times SF_{freq}$ spread chips per data symbol are involved in the 2-D spreading. The 2-D code assigned to the k^{th} user is denoted as $[c^{T(k)}, c^{F(k)}]$, where $c^{T(k)}$ is the time domain spreading code of length N and $c^{F(k)}$ is the frequency domain spreading sequence of length M.

At the transmitter, the bit stream of the k^{th} user during the j^{th} signal element, b_j^k, is first encoded, then mapped into symbols by the data modulator. The resultant symbol

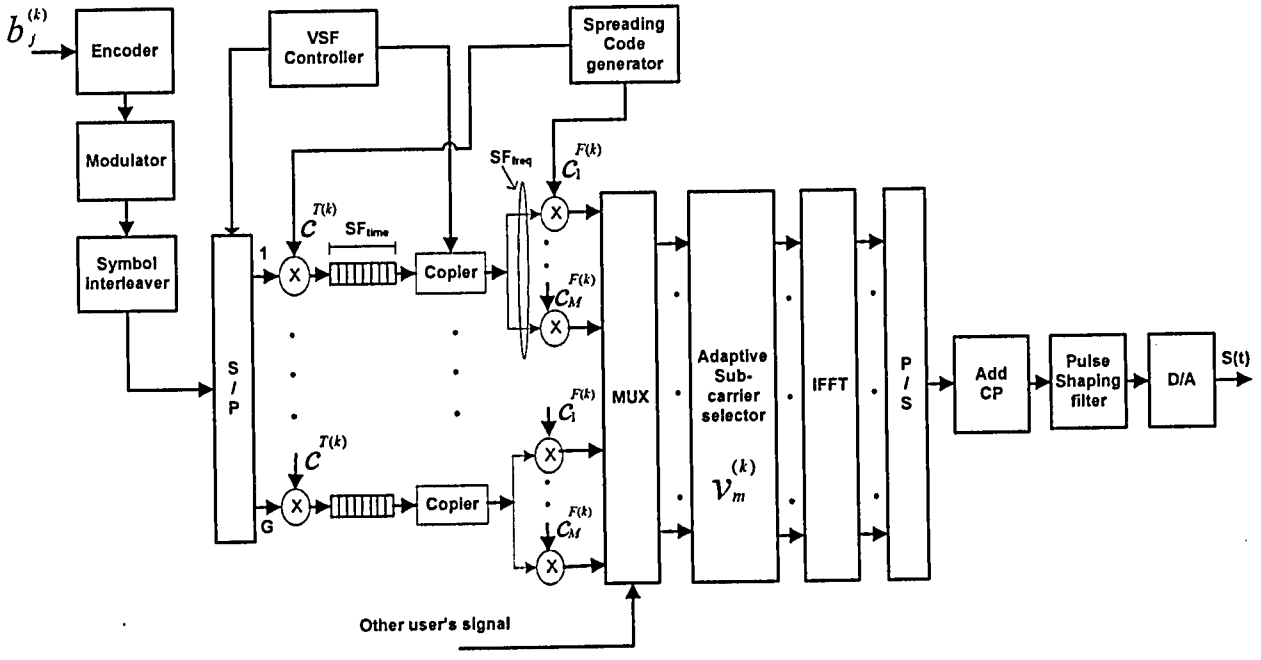

Figure 3.2: VSF-OFCDM transmitter.

sequence is then processed by the symbol interleaver [35]. The symbol interleaver has the same performance as the bit interleaver in OFCDM systems, but the former is simpler. A symbol interleaver is employed to separate successive symbols to non adjacent subcarriers to randomize the deep faded symbols due to frequency selective fading. Therefore, the frequency diversity can be achieved in frequency domain to improve the performance. Interleaved data symbols are then Serial-to-Parallel (S/P) converted into G substreams. After S/P conversion, 2-D spreading is carried out, where each data symbol is first spread into chips in time domain with the spreading code $c^{T(k)}$ and then the time-domain spread signal is duplicated into M copies and each copy is multiplied by a chip of the frequency domain spreading code $c^{F(k)}$. The spread signals from different users are added together by the multiplexer. An adaptive subcarrier selector block is then used that allows subcarriers to be selected adaptively based on the channel conditions. The parameters used by this block are determined by the adaptive subcarrier allocation algorithm [14] discussed later in section 3.2.3. The resultant signals are then up-converted into the selected subcarriers using an L point IFFT, where $L \geq M_c$ and

the value of L is a power of 2. The subcarriers are located in the middle of IFFT points and zeros are padded at each side of the M_c points. After IFFT, the OFCDM symbol is obtained. Then, a guard interval is inserted between OFCDM symbols to prevent ISI. Finally, the complete OFCDM symbol passes through a pulse shaping filter, which gives rise to the baseband transmitted signal.

Therefore, assuming BPSK modulation, the transmitted signal for the k^{th} user can be written as

$$s^{(k)}(t) = \sqrt{2P} \sum_{j} \sum_{g=1}^{G} b_{j,g}^{(k)} \sum_{l=1}^{M} v_{j,l,g}^{(k)} c_{j,l}^{F(k)} \cos(\omega_{l,g} t) \sum_{n=1}^{N} c_{j,l,n}^{T(k)} p(t - (jN + n)T_c), \tag{3.1}$$

where P is the transmitted power on one subcarrier. The bit stream of the k^{th} user on the g^{th} group during the j^{th} signal element, $b_{j,g}^{(k)}$, is equal to ± 1. $c_{j,l,n}^{T(k)}$ is the n^{th} chip in the time domain spreading code on the l^{th} subcarrier and $c_{j,l}^{F(k)}$ is the l^{th} chip in the frequency domain spreading sequence of length M during the j^{th} transmitted symbol. The parameter $v_{j,l,g}^{(k)} = 1$, if the l^{th} subcarrier of the g^{th} group is assigned to the k^{th} user by the adaptive subcarrier allocation algorithm [14]. If the l^{th} subcarrier of the g^{th} group is not assigned to user k, user k does not transmit data over this subcarrier and $v_{j,l,g}^{(k)} = 0$. $p(t)$ is the waveform of the pulse shaping filter and it is defined on the interval $[0, T_c]$, where T_c is the chip duration of the time domain spreading code, and it can be written as

$$P(t - (jN + n)T_c) = \begin{cases} 1, & (jN + n)T_c \le t \le (jN + n + 1)T_c; \\ 0, & \text{elsewhere.} \end{cases} \tag{3.2}$$

$\omega_{l,g}$ is the frequency of the l^{th} subcarrier of the g^{th} group and it can be written as

$$\omega_{l,g} = \omega_c + \frac{2\pi(g + (l-1)G)}{T_c}, \tag{3.3}$$

where ω_c is the carrier frequency and $1/T_c$ is the frequency spacing between two adjacent subcarriers.

3.2.2 Multipath Channel Model

In order to consider a realistic radio propagation channel, we must include the effects of the multipath propagation. Before introducing the impulse response of the channel used in our analysis, we will discuss briefly the effect of multipath on the received signal.

Small Scale Propagation Models

Small scale propagation models predict the fluctuations in the received signal strength. The received signal is composed of several time delayed versions of the transmitted signal. These signals add at the receiver with different phases as a result of different propagation delays. Fading is classified into different types. Based on the multipath time delay spread, fading can be flat or frequency selective and depending on Doppler spread, they can be fast or slow fading since the Doppler spread is a measure of the spectral broadening caused by the time rate of change of the mobile radio channel. Flat fading occurs when the bandwidth of the signal is smaller than the bandwidth of the channel. It is sometimes known as slowly varying channel or narrowband channel. In flat fading, the delay spread is also less than the symbol period. Flat fading channels are modeled as Rayleigh or Ricean distributed channels.

When the delay spread is greater than the symbol period, there are multiple versions of the transmitted signal at the receiver and the received signal is attenuated and differs in phase. This is called frequency selective fading where the bandwidth of the signal is greater than the bandwidth of the channel which results in ISI. These channels are widely known as wideband channels and are modeled as Two-Ray Rayleigh models [36].

Factors contributing to small scale fading include multipath propagation, mobile velocity, and the transmission bandwidth of the signal.

Doppler Effect

Fading is also caused by the Doppler effect. When dealing with any kind of waves, a receiver movement in relation to the source of the wave will distort the perceived frequency of that wave. Doppler shift is the frequency shift in the received signal caused due to the relative motion between the transmitter and the receiver. This phase change is given by [37]

$$f_D = \frac{v}{c} f_c \cos(\theta), \tag{3.4}$$

where f_D is the Doppler shift in frequency, v is the velocity, c is the speed of light, f_c is the carrier frequency, and θ is the angle between the transmitter and the receiver. If the signal bandwidth is much greater than the Doppler spread, which is defined as the difference between the largest and the smallest Doppler shifts, then the effect of the Doppler spread is negligible at the receiver.

The coherence time of the channel, T_{ch}, is the time duration over which the channel impulse response is essentially invariant. The relation between the Doppler spread and the coherence time of the channel is given by [37]

$$T_{ch} = \frac{0.423}{f_{DS}}, \tag{3.5}$$

where f_{DS} is the Doppler spread.

The Channel Model

In our analysis, we assume that the channel is slowly varying with respect to the OFCDM symbol duration, T_s. This is a valid assumption because the Doppler spread is generally much smaller than the subcarrier bandwidth. We also assume that the chip duration (T_c) is equivalent to the RMS delay spread of the channel. Therefore, each subcarrier experiences independent, frequency non-selective fading and the channel is modeled as a Rayleigh fading

channel. A simple way to model the Rayleigh fading effect is the quasi-static assumption where the channel is assumed to be constant over a block period of time which in our case is the chip duration T_c. In this model, we generate a Rayleigh random variable and a complex exponential with a uniform phase and multiply it with the transmitted signal and then compensate for this distortion at the receiver. Hence, the impulse response of the channel for the k^{th} user and the l^{th} subcarrier of the g^{th} group can be described as [26]

$$h_{l,g}^{(k)}(t,j) = \alpha_{l,g}^{(k)}(t,j)e^{i(\phi_{l,g}^{(k)})}, \tag{3.6}$$

where $\alpha_{l,g}^{(k)}$ are independent identically distributed (i.i.d.) Rayleigh random variables for the k^{th} user on the l^{th} subcarrier of the g^{th} group during the j^{th} transmitted OFCDM symbol. The phase, $\phi_{l,g}^{(k)}$, is a uniformly distributed random variable over the interval [0, 2π), which is independent for each symbol, subcarrier and user. Furthermore, the channel fading and phase shift variables are considered to be constant over a chip duration T_c.

The received signal is a sum of all the K users' signals transmitted during the j^{th} signal element. These signals are all corrupted by independent fading conditions, as well as Additive White Gaussian Noise (AWGN). Consequently, the received signal is expressed as

$$r(t) = \sum_{k=1}^{K} s^{(k)}(t) * h^{(k)}(t) + n(t), \tag{3.7}$$

where $h^{(k)}(t)$ represents the total impulse response across all subcarriers for user k, $n(t)$ is the AWGN with zero mean and double-sided power spectral density $N_0/2$ and $(*)$ denotes the convolution process.

3.2.3 Adaptive Subcarrier Allocation in OFCDM

Various adaptive subcarrier allocation algorithms were proposed for MC-CDMA and MC-DS-CDMA systems [12]. Many of these algorithms outperform the corresponding non-adaptive systems in terms of the BER performance. In OFCDM systems, an adaptive subcarrier

allocation algorithm was proposed to maximize the overall BER performance under different spreading factors [14]. In this algorithm, the total spectrum is separated into small groups of non-contiguous subcarriers to maximize frequency diversity gains and minimize MAI as mentioned earlier. The users are assigned to subcarriers based on the instantaneous Signal to Interference and Noise Ratio (SINR) characteristics of each subcarrier such that the average SINR of the system is maximized while minimizing the interference caused to other users simultaneously.

The flowchart for the adaptive subcarrier allocation algorithm is shown in Fig. 3.3 for the sake of completeness (taken from [14]); the algorithm can be summarized in the following steps :

Step 1: Determine the fading gain $\alpha_{m,g}^{(k)}$ on the m^{th} subcarrier of the g^{th} group for all K users, where $k = 1, 2, 3..., K$.

Step 2: Calculate the SINR $\gamma_g^{(k)}$ of each group g for all K users. At the beginning of the algorithm, the interference power is null, therefore, SINR simplifies to SNR as:

$$\gamma_g^{(k)} = \frac{2PN \sum_{m=1}^{M} (\alpha_{m,g}^{(k)})^2}{N_o}, \tag{3.8}$$

where M is the total number of subcarriers in group g, N is the length of the time domain spreading code and N_o is the noise power density.

Step 3: Define the set $Q = \{\beta^{(1)}, \beta^{(2)}, \ldots, \beta^{(K)}\}$ where $\beta^{(k)}$ is the maximum number of substreams that can be transmitted by the k^{th} user.

Step 4: Find the subcarrier group that has the largest $\gamma_g^{(k)}$ for all K users, $\gamma_{max}^{(k)}$, and record the index of the subcarrier group that produces the largest value for all K users $g_{max}^{(k)}$.

Step 5: Find the smallest value in the set $\gamma_{max}^{(k)}$ denoted by γ_{min}. This corresponds to the subcarrier group with the best fading gain, which causes the lowest amount of MAI to other users. The user with the lowest SINR value is denoted by k_{min}.

Step 6: Assign user k_{min} to the subcarrier group $g_{max}^{(k_{min})}$. This effectively assigns the

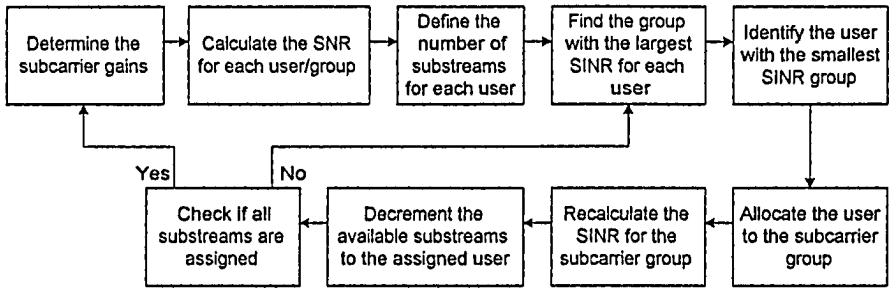

Figure 3.3: Adaptive Subcarrier Allocation Flowchart.

subcarrier group with the highest SINR for user k_{min}. Since it is the smallest value in the set $\gamma_{max}^{(k)}$, it minimizes the interference to other users.

Step 7: Recalculate the SINR for the subcarrier group that corresponds to $g_{max}^{(k_{min})}$. The SINR is recalculated by incrementing the number of users occupying group g simultaneously, K_g, to reflect the additional user occupying the subcarrier group g according to the equation:

$$\gamma_g^{(1)} = \frac{2NPT_c \sum_{m=1}^{M} (\alpha_{m,g}^{(1)})^2}{(K_g - 1)PT_c E[(\alpha_{m,g}^{(k)})^2] + N_o}, \tag{3.9}$$

where $E[(\alpha_{m,g}^{(k)})^2]$ is the average squared fading gain for the K_g users and the M subcarriers in group g.

Step 8: Decrement the number of available substreams for user k_{min}. The process of assigning substreams to subcarriers continues recursively until all substreams are assigned to subcarriers. Therefore, if the entire set $Q = 0$, return to Step 1 where the next set of subcarriers is assigned (the next update period), otherwise return to Step 4.

Throughout the remainder of this thesis, we will consider the VSF-OFCDM system where different subcarriers are allocated to different users according to the adaptive subcarrier allocation algorithm discussed above.

3.2.4 VSF-OFCDM Receiver

The VSF-OFCDM receiver block diagram is shown in Fig. 3.4. Assuming BPSK modulation, the received signal is given by

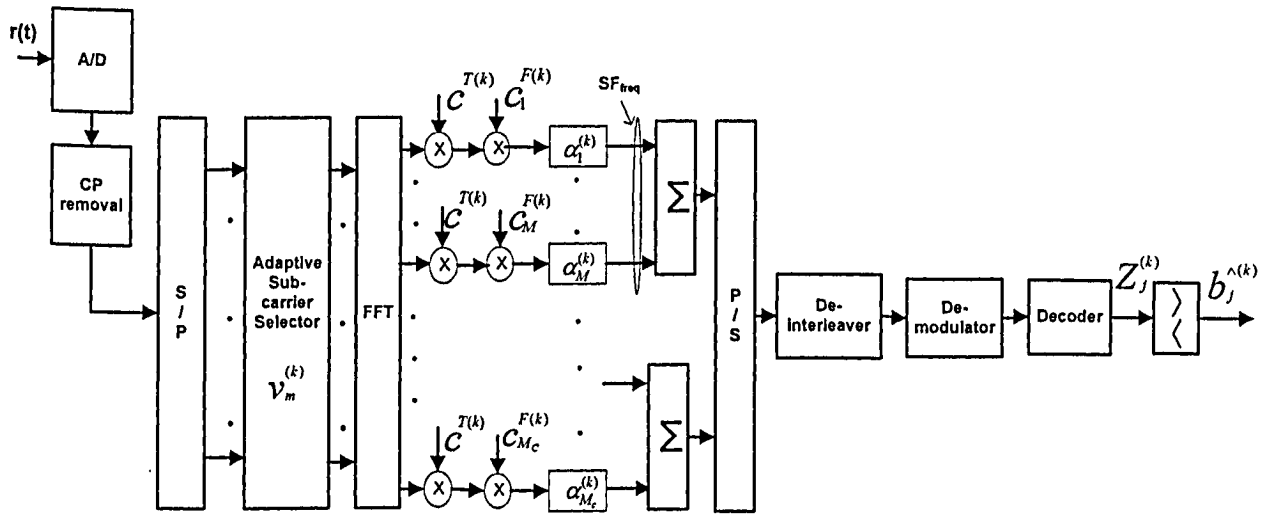

Figure 3.4: VSF-OFCDM receiver for user k.

$$r(t) = \sqrt{2P} \sum_{j} \sum_{g=1}^{G} \sum_{k=1}^{K_g} b_{j,g}^{(k)} \sum_{l=1}^{M} \alpha_{l,g}^{(k)} c_{j,l}^{F(k)} \cos(\omega_{l,g} t + \phi_{l,g}^{(k)}) \sum_{n=1}^{N} c_{j,l,n}^{T(k)} p(t - (jN + n)T_c) + n(t), \tag{3.10}$$

where K_g is the total number of users in group g, $b_{j,g}^{(k)}$ is the BPSK signal for the k^{th} user in the g^{th} group during the j^{th} transmitted bit.

Assuming that the guard interval is larger than the maximum path delay spread, there is no ISI in the received signals. Without loss of generality, we aim to recover the data transmitted to user 1 in group 1. We first convert the received signal into parallel format using the serial-to-parallel converter and then multiply by the subcarrier allocation coefficients for user 1, $v_{m,1}^{(1)}$. This ensures that only the allocated subcarriers are detected at the receiver. Following this, the signal on each subcarrier is down-converted by the FFT block. We then correlate the received signal with the synchronized time and frequency domain spreading

sequences for user 1, $[c^{T(1)}, c^{F(1)}]$. The signal on the m^{th} subcarrier is first correlated with the synchronized time domain spreading sequence for user 1, $c^{T(1)}$. The output of each time domain correlator is then multiplied by a chip from the frequency domain spreading code of user 1, $c^{F(1)}$, to remove the frequency domain spreading. The output is then combined at the frequency domain despreader and multiplied by the path weight for the corresponding subcarrier. The receiver uses the Maximal Ratio Combining (MRC) algorithm to maximize the SNR at the output of the correlator. In this combining algorithm, the weight given to the m^{th} subcarrier in group 1 is equivalent to the fading gain on this subcarrier, $\alpha_{m,1}^{(1)}$. After Parallel-to-Serial (P/S) conversion, the output is demodulated, decoded and sampled to yield the decision variable for the k^{th} user at the j^{th} transmitted signal. The decision variable for user 1 in group 1 is given by

$$z_{j,1}^{(1)} = \sum_{m=1}^{M} \sum_{n=1}^{N} \frac{1}{T_c} \int_{(jN+n)T_c}^{(jN+n+1)T_c} \alpha_{m,1}^{(1)} c_{j,m}^{F(1)} c_{j,m,n}^{T(1)} r(t) \cos(\omega_{m,1} t + \hat{\phi}_{m,1}^{(1)}) dt, \qquad (3.11)$$

where $\hat{\phi}_{m,1}^{(1)}$ denotes the estimated phase of the m^{th} subcarrier of group 1 during the j^{th} transmitted bit to user 1.

In chapter 4 and 5, we will focus our study on enhancing the performance of the VSF-OFCDM system through mitigating the effect of carrier frequency offset and applying adaptive modulation.

Chapter 4

Carrier Frequency Offset in VSF-OFCDM Systems: Analysis and Correction

In this chapter, we investigate the effect of Carrier Frequency Offset (CFO) on the performance of downlink VSF-OFCDM systems and propose a scheme for its correction. First, we analyze the BER of VSF-OFCDM taking into account the effect of frequency offset when subcarrier grouping is used. This leads to an analytic expression of the SINR for VSF-OFCDM with frequency offset when using BPSK modulation for the case of MRC receiver. Following this, we propose a CFO correction scheme based on the Maximum Likelihood (ML) estimation principle. After deriving the likelihood function for the VSF-OFCDM system with CFO, we use a gradient algorithm to estimate and minimize the effect of CFO in a tracking mode.

4.1 Effect of CFO on VSF-OFCDM Systems

One of the main drawbacks of multicarrier systems is that they suffer a great deal of performance degradation from CFO. Frequency offset causes a loss of orthogonality between

subcarriers which results in Intercarrier Interference (ICI). The impact of frequency offset on multicarrier systems was investigated in [15] and [16] for MC-CDMA and group-orthogonal MC-CDMA respectively, and in [17] for both uplink and downlink MC-DS-CDMA systems. Recently, there are few papers investigating the effect of frequency offset on OFCDM systems. In [38], the BER performance of multiple antenna OFCDM systems with imperfections was studied. In [27], the sensitivity of OFDM-CDMA systems to carrier frequency offset was investigated for zero forcing and minimum mean square error equalizers. However, no subcarrier grouping was considered in their analysis, although this strategy has an impact on the different types and amount of interference introduced with carrier frequency offset. Also, the effect of using variable spreading factors on the BER performance of OFCDM systems was not investigated in their work.

The two major factors that cause carrier frequency offset are the Doppler spread caused in the channel for a high speed mobile user and the differences between the oscillators in the transmitter and the receiver. In our work, the effect of the frequency offset is analyzed by investigating the type and the amount of interference caused by CFO in VSF-OFCDM systems with different spreading factors when subcarrier grouping is used. We assume BPSK modulation throughout this chapter so no adaptive modulation is used here.

4.1.1 Bit Error Rate Analysis

In this section, an analytic expression of the SINR for downlink VSF-OFCDM with frequency offset using BPSK modulation is derived for the case of MRC receiver. The central limit theorem implies that the contribution of a large number of identically distributed chips of interference will tend towards a Gaussian distribution. Therefore, in our analysis, the standard Gaussian approximation [39] is applied to the interference and noise terms.

The Doppler shift caused in the channel for a high speed mobile user results in a carrier frequency offset which is different for each subcarrier according to where it is located in the spectrum. However in a 4G system [3], the maximum Doppler spread is very small with

respect to the subcarrier spacing, therefore, we can consider the CFO caused by the Doppler shift a common phenomenon in all the subcarriers [15]. We also assume that each subcarrier experiences independent, frequency nonselective fading. Furthermore, the channel fading and phase shift variables are considered to be constant over a chip duration T_c as mentioned earlier.

Taking into account the frequency offset for the k^{th}, $f_d^{(k)}$, the impulse response of the channel for the k^{th} user and the l^{th} subcarrier of the g^{th} group during the j^{th} transmitted bit can be described as [26]:

$$h_{l,g}^{(k)}(t,j) = \alpha_{l,g}^{(k)}(t,j)e^{i(2\pi f_d^{(k)}t+\phi_{l,g}^{(k)})}. \tag{4.1}$$

Therefore, the received signal with CFO assuming BPSK modulation, can be written as

$$r(t) = \sqrt{2P}\sum_{j}\sum_{g=1}^{G}\sum_{k=1}^{K_g} b_{j,g}^{(k)}\sum_{l=1}^{M}\alpha_{l,g}^{(k)}c_{j,l}^{F(k)}\cos(\omega_{l,g}t+\phi_{l,g}^{(k)}+\omega_d^{(k)}t)\sum_{n=1}^{N}c_{j,l,n}^{T(k)}p(t-(jN+n)T_c)+n(t), \tag{4.2}$$

Since we consider MRC in our analysis, the decision variable for user 1 in group 1 is given by (3.11). For simplicity of further calculations, the decision variable can be expressed as

$$z_{j,1}^{(1)} = S+\eta+MAI+ICI_1+ICI_2+ICI_g, \tag{4.3}$$

where S is the desired signal term; η is the noise term; MAI represents the multiple access interference imposed by the interfering users in the same group of the desired user from the same subcarriers, where the considered subcarriers are $m = 1,\cdots,M$; ICI_1 is the self-intercarrier interference from the other subcarriers of the same group; ICI_2 is the multiple access intercarrier interference imposed by the interfering users in the same group of the desired user, but associated with the subcarriers different from the considered subcarrier and ICI_g is the intergroup interference which represents the intercarrier interference from subcarriers in other groups. Without loss of generality, these parameters are considered for

user 1 in group 1 at the j^{th} transmitted bit.

The desired signal term can be written as

$$S = \frac{1}{T_c}\sqrt{\frac{P}{2}} b_{j,1}^{(1)} \sum_{m=1}^{M} \left(\alpha_{m,1}^{(1)}\right)^2 [c_{j,m}^{F(1)} c_{j,m}^{F(1)}] \times \sum_{n=1}^{N} \int_{(jN+n)T_c}^{(jN+n+1)T_c} [c_{j,m,n}^{T(1)} c_{j,m,n}^{T(1)}] p(t-(jN+n)T_c) \cos(\omega_d^{(1)} t + \phi_{m,1}^{(1)} - \hat{\phi}_{m,1}^{(1)}) dt. \tag{4.4}$$

The rectangular function, $p(t-(jN+n)T_c)$, has a constant amplitude of unity over T_c and since $b_{j,1}^{(1)}$, $[c_{j,m}^{F(1)} c_{j,m}^{F(1)}]$ and $\left(\alpha_{j,m}^{(1)}\right)^2$ are constants over T_c, they can be taken outside the integral. In addition, since the system spreading codes are synchronized at the receiver, $[c_{j,m}^{F(1)} c_{j,m}^{F(1)}] = 1$ and $[c_{j,m,n}^{T(1)} c_{j,m,n}^{T(1)}] = 1$ and the desired signal term can be re-written as

$$S = \sqrt{\frac{P}{2}} b_{j,1}^{(1)} \frac{\sin\left(\frac{\omega_d^{(1)} T_c}{2}\right)}{\left(\frac{\omega_d^{(1)} T_c}{2}\right)} \sum_{m=1}^{M} \left(\alpha_{m,1}^{(1)}\right)^2 \sum_{n=1}^{N} \cos\left((jN+n+1/2)\omega_d^{(1)} T_c + \phi_{m,1}^{(1)} - \hat{\phi}_{m,1}^{(1)}\right). \tag{4.5}$$

The noise term can be written as

$$\eta = \frac{1}{T_c} \sum_{m=1}^{M} \alpha_{m,1}^{(1)} c_{j,m}^{F(1)} \sum_{n=1}^{N} c_{j,m,n}^{T(1)} \int_{(jN+n)T_c}^{(jN+n+1)T_c} p(t-(jN+n)T_c) n(t) \cos(\omega_{m,1} t + \hat{\phi}_{m,1}^{(1)}) dt. \tag{4.6}$$

The noise term η is a Gaussian random variable with zero mean and variance given by

$$\sigma_\eta^2 = E[\eta^2] = \frac{NN_0}{4T_c} \sum_{m=1}^{M} \left(\alpha_{m,1}^{(1)}\right)^2. \tag{4.7}$$

The interference term MAI is obtained from (3.11) with the condition that $g = 1$ and $l = m$ for $k \neq 1$. It can be expressed as

$$MAI = \frac{1}{T_c}\sqrt{\frac{P}{2}} \sum_{k=2}^{K_1} b_{j,1}^{(k)} \sum_{m=1}^{M} \alpha_{m,1}^{(1)} \alpha_{m,1}^{(k)} c_{j,m}^{F(1)} c_{j,m}^{F(k)} \times \sum_{n=1}^{N} \int_{(jN+n)T_c}^{(jN+n+1)T_c} c_{j,m,n}^{T(1)} c_{j,m,n}^{T(k)} p(t-(jN+n)T_c) \cos(\omega_d^{(k)} t + \phi_{m,1}^{(k)} - \hat{\phi}_{m,1}^{(1)}) dt, \tag{4.8}$$

where K_1 is the total number of users in group 1.

The MAI term can be re-written as

$$MAI = \sqrt{\frac{P}{2}} \sum_{k=2}^{K_1} \sum_{m=1}^{M} \sum_{n=1}^{N} b_{j,1}^{(k)} \frac{\sin\left(\frac{\omega_d^{(k)} T_c}{2}\right)}{\left(\frac{\omega_d^{(k)} T_c}{2}\right)} \alpha_{m,1}^{(1)} \alpha_{m,1}^{(k)} c_{j,m}^{F(1)} c_{j,m}^{F(k)} \times c_{j,m,n}^{T(1)} c_{j,m,n}^{T(k)} \cos\left((jN + n + 1/2)\omega_d^{(k)} T_c + \phi_{m,1}^{(k)} - \hat{\phi}_{m,1}^{(1)}\right). \tag{4.9}$$

According to the central limit theorem, the MAI can be approximated by a Gaussian random variable with zero mean and variance given by

$$\sigma_{MAI}^2 = N\frac{P}{4}(K_1 - 1)E\left[(\alpha_{m,1}^{(k)})^2 \frac{\sin^2\left(\frac{\omega_d^{(k)} T_c}{2}\right)}{\left(\frac{\omega_d^{(k)} T_c}{2}\right)^2}\right] \sum_{m=1}^{M} (\alpha_{m,1}^{(1)})^2, \tag{4.10}$$

where $\phi_{m,1}^{(k)}$ and $\hat{\phi}_{m,1}^{(1)}$ are i.i.d. random variables uniformly distributed over the interval $[0, 2\pi)$. The term $[(jN + n + 1/2)\omega_d^{(k)} T_c]$ only rotates the phase $[\phi_{m,1}^{(k)} - \hat{\phi}_{m,1}^{(1)}]$; therefore, $E[\cos^2((jN + n + 1/2)\omega_d^{(k)} T_c + \phi_{m,1}^{(k)} - \hat{\phi}_{m,1}^{(1)})] = \frac{1}{2}$.

The self-intercarrier interference term ICI_1 can be obtained from (3.11) by letting $k = 1$, $g = 1$ and $l \neq m$. It can be written as

$$ICI_1 = \frac{1}{T_c}\sqrt{\frac{P}{2}} b_{j,1}^{(1)} \sum_{m=1}^{M} \sum_{\substack{l=1 \\ l \neq m}}^{M} \alpha_{m,1}^{(1)} \alpha_{l,1}^{(1)} c_{j,m}^{F(1)} c_{j,l}^{F(1)} \times \sum_{n=1}^{N} \int_{(jN+n)T_c}^{(jN+n+1)T_c} c_{j,m,n}^{T(1)} c_{j,l,n}^{T(1)} p(t - (jN + n)T_c) \cos((\omega_d^{(1)} + \omega_{l,1} - \omega_{m,1})t + \phi_{l,1}^{(1)} - \hat{\phi}_{m,1}^{(1)}) dt, \tag{4.11}$$

which can be re-written as

$$ICI_1 = \sqrt{\frac{P}{2}} b_{j,1}^{(1)} \sum_{m=1}^{M} \sum_{\substack{l=1 \\ l \neq m}}^{M} \sum_{n=1}^{N} \frac{\sin\left(\frac{\omega_d^{(1)} T_c}{2}\right)}{\left(\frac{(\omega_d^{(1)} + \omega_{l,1} - \omega_{m,1}) T_c}{2}\right)}$$
$$\times \alpha_{m,1}^{(1)} \alpha_{l,1}^{(1)} c_{j,m}^{F(1)} c_{j,l}^{F(1)} c_{j,m,n}^{T(1)} c_{j,l,n}^{T(1)} \cos\left((jN + n + 1/2)(\omega_d^{(1)} + \omega_{l,1} - \omega_{m,1}) T_c + \phi_{l,1}^{(1)} - \hat{\phi}_{m,1}^{(1)}\right). \tag{4.12}$$

The ICI_1 can be approximated by a Gaussian random variable with zero mean and variance given by

$$\sigma_{ICI_1}^2 = N \frac{P}{4} \sum_{m=1}^{M} \left(\alpha_{m,1}^{(1)}\right)^2 \sum_{\substack{l=1 \\ l \neq m}}^{M} \left(\alpha_{l,1}^{(1)}\right)^2 \frac{\sin^2\left(\frac{\omega_d^{(1)} T_c}{2}\right)}{\left(\frac{(\omega_d^{(1)} + \omega_{l,1} - \omega_{m,1}) T_c}{2}\right)^2}. \tag{4.13}$$

The multiple access interference from users in the same group as the desired user, but associated with the subcarriers different from the considered subcarrier, ICI_2, is obtained by setting $k \neq 1$, $g = 1$ and $l \neq m$ in (3.11). It can be written as

$$ICI_2 = \frac{1}{T_c} \sqrt{\frac{P}{2}} \sum_{k=2}^{K_1} b_{j,1}^{(k)} \sum_{m=1}^{M} \sum_{\substack{l=1 \\ l \neq m}}^{M} \alpha_{m,1}^{(1)} \alpha_{l,1}^{(k)} c_{j,m}^{F(1)} c_{j,l}^{F(k)}$$
$$\times \sum_{n=1}^{N} \int_{(jN+n)T_c}^{(jN+n+1)T_c} c_{j,m,n}^{T(1)} c_{j,l,n}^{T(k)} p(t - (jN + n)T_c) \cos((\omega_d^{(k)} + \omega_{l,1} - \omega_{m,1})t + \phi_{l,1}^{(k)} - \hat{\phi}_{m,1}^{(1)}) dt, \tag{4.14}$$

which can be re-written as

$$ICI_2 = \sqrt{\frac{P}{2}} \sum_{k=2}^{K_1} \sum_{m=1}^{M} \sum_{\substack{l=1 \\ l \neq m}}^{M} \sum_{n=1}^{N} b_{j,1}^{(k)} \frac{\sin\left(\frac{\omega_d^{(k)} T_c}{2}\right)}{\left(\frac{(\omega_d^{(k)} + \omega_{l,1} - \omega_{m,1}) T_c}{2}\right)}$$
$$\times \alpha_{m,1}^{(1)} \alpha_{l,1}^{(k)} c_{j,m}^{F(1)} c_{j,m,n}^{T(1)} c_{j,l}^{F(k)} c_{j,l,n}^{T(k)} \cos\left((jN + n + 1/2)(\omega_d^{(k)} + \omega_{l,1} - \omega_{m,1}) T_c + \phi_{l,1}^{(k)} - \hat{\phi}_{m,1}^{(1)}\right). \tag{4.15}$$

The ICI_2 can be approximated by a Gaussian random variable with zero mean and variance given by

$$\sigma^2_{ICI_2} = N(K_1 - 1)\frac{P}{4}\sum_{m=1}^{M}\left(\alpha^{(1)}_{m,1}\right)^2 E\left[\left(\alpha^{(k)}_{l,1}\right)^2 \frac{\sin^2\left(\frac{\omega_d^{(k)}T_c}{2}\right)}{\left(\frac{(\omega_d^{(k)}+\omega_{l,1}-\omega_{m,1})T_c}{2}\right)^2}\right]. \tag{4.16}$$

The interference from other groups ICI_g can be obtained from (3.11) by letting $g \neq 1$ and can be expressed as

$$ICI_g = \frac{1}{T_c}\sqrt{\frac{P}{2}}\sum_{g=2}^{G}\sum_{k=1}^{K_g} b^{(k)}_{j,g}\sum_{m=1}^{M}\sum_{l=1}^{M}\alpha^{(1)}_{m,1}\alpha^{(k)}_{l,g}c^{F(1)}_{j,m}c^{F(k)}_{j,l}$$
$$\times\sum_{n=1}^{N}\int_{(jN+n)T_c}^{(jN+n+1)T_c} c^{T(1)}_{j,m,n}c^{T(k)}_{j,l,n}p(t-(jN+n)T_c)\cos((\omega_d^{(k)}+\omega_{l,g}-\omega_{m,1})t+\phi^{(k)}_{l,g}-\hat{\phi}^{(1)}_{m,1})dt, \tag{4.17}$$

which can be re-written as

$$ICI_g = \sqrt{\frac{P}{2}}\sum_{g=2}^{G}\sum_{k=1}^{K_g}\sum_{m=1}^{M}\sum_{l=1}^{M}\sum_{n=1}^{N} b^{(k)}_{j,g}\frac{\sin\left(\frac{\omega_d^{(k)}T_c}{2}\right)}{\left(\frac{(\omega_d^{(k)}+\omega_{l,g}-\omega_{m,1})T_c}{2}\right)}$$
$$\times\alpha^{(1)}_{m,1}\alpha^{(k)}_{l,g}c^{F(1)}_{j,m}c^{T(1)}_{j,m,n}c^{F(k)}_{j,l}c^{T(k)}_{j,l,n}\cos\left((jN+n+1/2)(\omega_d^{(k)}+\omega_{l,g}-\omega_{m,1})T_c+\phi^{(k)}_{l,g}-\hat{\phi}^{(1)}_{m,1}\right). \tag{4.18}$$

The ICI_g can be approximated by a Gaussian random variable with zero mean and variance given by

$$\sigma^2_{ICI_g} = N\frac{P}{4}\sum_{g=2}^{G}K_g\sum_{m=1}^{M}\left(\alpha^{(1)}_{m,1}\right)^2 E\left[\left(\alpha^{(k)}_{l,g}\right)^2 \frac{\sin^2\left(\frac{\omega_d^{(k)}T_c}{2}\right)}{\left(\frac{(\omega_d^{(k)}+\omega_{l,g}-\omega_{m,1})T_c}{2}\right)^2}\right]. \tag{4.19}$$

If we assume the frequency offset is equal and constant for all users [15, 16], therefore, $\omega_d^{(k)} = \omega_d$. Also, we can assume the estimated phase for user 1 in group 1 to be $\hat{\phi}^{(1)}_{m,1} = (jN+n+1/2)\omega_d T_c + \phi^{(1)}_{m,1}$ [40]. This means that the subcarrier phase estimator determines

the value of the phase rotation at time $(n+1/2)T_c$ which is the middle of the n^{th} chip integration interval. The desired signal term in (4.5) becomes

$$S = N\sqrt{\frac{P}{2}}b_{j,1}^{(1)}\frac{\sin\left(\frac{\omega_d T_c}{2}\right)}{\left(\frac{\omega_d T_c}{2}\right)}\sum_{m=1}^{M}\left(\alpha_{m,1}^{(1)}\right)^2. \tag{4.20}$$

In our analysis, we consider downlink transmission; therefore, we can assume that all the users suffer equal fading gain and phase shift on each subcarrier [16], which means that $\alpha_{m,g}^{(k)} = \alpha_{m,g}$, and we can further simplify (4.7), (4.10), (4.13), (4.16) and (4.19) as follows

$$\sigma_\eta^2 = \frac{NN_0}{4T_c}\sum_{m=1}^{M}(\alpha_{m,1})^2, \tag{4.21}$$

$$\sigma_{MAI}^2 = N\frac{P}{4}(K_1-1)\frac{\sin^2(\pi f_d T_c)}{(\pi f_d T_c)^2}\sum_{m=1}^{M}(\alpha_{m,1})^4, \tag{4.22}$$

$$\sigma_{ICI_1}^2 = N\frac{P}{4\pi^2}\sin^2(\pi f_d T_c)\sum_{m=1}^{M}(\alpha_{m,1})^2\sum_{\substack{l=1\\ l\neq m}}^{M}\frac{(\alpha_{l,1})^2}{(f_d T_c+(l-m)G)^2}, \tag{4.23}$$

$$\sigma_{ICI_2}^2 = N(K_1-1)\frac{P}{4\pi^2}\sin^2(\pi f_d T_c)\sum_{m=1}^{M}(\alpha_{m,1})^2\sum_{\substack{l=1\\ l\neq m}}^{M}\frac{(\alpha_{l,1})^2}{(f_d T_c+(l-m)G)^2}, \tag{4.24}$$

$$\sigma_{ICI_g}^2 = N\frac{P}{4\pi^2}\sin^2(\pi f_d T_c)\sum_{g=2}^{G}\sum_{m=1}^{M}\sum_{l=1}^{M}\frac{K_g(\alpha_{l,g})^2(\alpha_{m,1})^2}{\Big(f_d T_c+(g-1)+(l-m)G\Big)^2}. \tag{4.25}$$

The signal to noise and interference (SINR) of user 1 in group 1 during the j^{th} bit can be expressed as

$$\gamma_{j,1}^{(1)} = \frac{E^2[S]}{\sigma_{MAI}^2+\sigma_{ICI_1}^2+\sigma_{ICI_2}^2+\sigma_{ICI_g}^2+\sigma_\eta^2}, \tag{4.26}$$

where

$$E^2[S] = \frac{N^2P}{2}\frac{\sin^2(\pi f_d T_c)}{(\pi f_d T_c)^2}\left[\sum_{m=1}^{M}(\alpha_{m,1})^2\right]^2. \tag{4.27}$$

The probability of error for MRC based on the Gaussian assumption for BPSK modulation can be expressed as

$$P_e = \mathrm{Q}\left(\sqrt{2\gamma_{j,1}^{(1)}}\right), \tag{4.28}$$

where Q(.) is the Q function,

$$\mathrm{Q(x)} = \frac{1}{2\pi}\int_x^\infty e^{\frac{-x^2}{2}}dx. \tag{4.29}$$

4.1.2 Numerical Results

The parameters chosen for the VSF-OFCDM system correspond to those expected in a 4G system [3]. The carrier frequency, f_c, is 5 GHz and the downlink channel bandwidth is 100 MHz. There are 128 subcarriers and we assume that each subcarrier experiences frequency non-selective fading and that fading is uncorrelated between subcarriers in the same group as a result of the subcarrier grouping strategy used. In our evaluation, we assume a delay spread which is identical to the chip duration, T_c, indicating there is no ISI produced by the channel. This allows us to use independent, identically distributed Rayleigh variables to represent the gain of each subcarrier. The maximum difference in Doppler spread between the subcarriers is in the range of 0-5Hz which is very small compared to the subcarrier spacing. The update period of the adaptive subcarrier allocation algorithm is selected to be equivalent to the coherence time of the channel to ensure that the channel is constant over the update period [14]. In OFCDM, each data stream is segmented into multiple substreams and spread over multiple subcarriers and several OFCDM symbols as mentioned before. We use an identical data rate for each user in each analysis by transmitting a number of substreams equal to a multiple of the number of chips in the time domain spreading code N. In this evaluation, we transmit $2N$ substreams simultaneously for each user.

The different spreading factors can be used to provide different levels of frequency diversity, or to minimize MAI in the event of high channel loads. SF_{time} is equal to the N chips in the time domain spreading code and SF_{freq} is equal to the M subcarriers in each

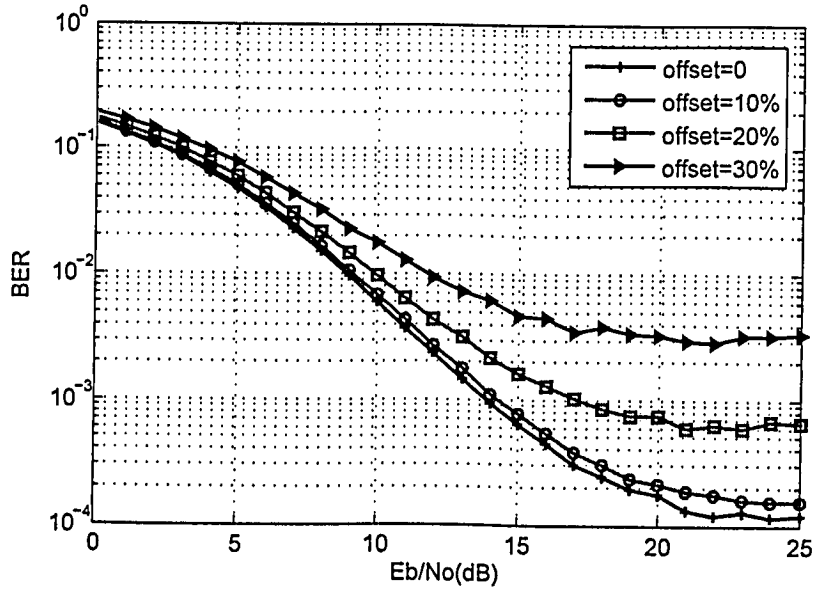

Figure 4.1: BER vs. E_b/N_o with SF=2x16 at different normalized frequency offsets.

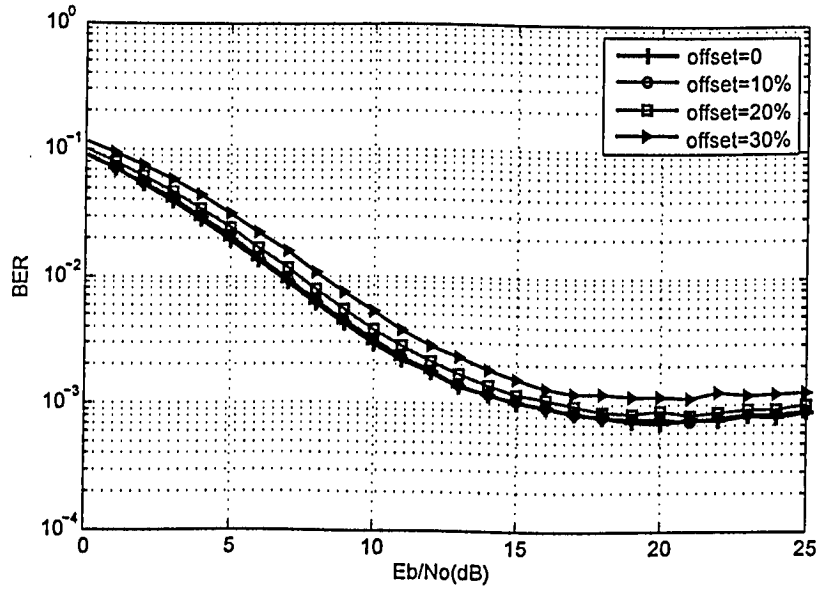

Figure 4.2: BER vs. E_b/N_o with SF=16x2 at different normalized frequency offsets.

group g. We consider a VSF-OFCDM system with 16 users, having carrier frequency offsets of 0, 10, 20 and 30% of the frequency spacing between adjacent subcarriers. Each of the configurations uses a total spreading factor $SF = SF_{time} \times SF_{freq}$ of 32 to provide a suitable

performance comparison. We use a total SF of 2x16 to represent a case with high frequency domain spreading and 16x2 to represent a case with high time domain spreading respectively. We also use a total SF of 8x4 and 4x8 to represent cases of using moderate levels of time and frequency domain spreading for VSF-OFCDM systems.

The effect of carrier frequency offset on the mean BER performance with different spreading factors is investigated by using Monte-Carlo simulation with 1000 runs and with the above mentioned parametric values. Figs. 4.1 and 4.2 show the BER vs. E_b/N_o with total SF of 2x16 and 16x2 respectively. It can be observed from these figures that the degradation in BER caused by carrier frequency offset is insignificant at very low E_b/N_o. However, as E_b/N_o increases the OFCDM system makes a transition from being noise-limited to being interference-limited, and the degree of degradation increases as well. It can also be seen from the figures that the degradation in BER caused by the carrier frequency offset increases with higher SF_{freq} because of the fact that more subcarriers are present in each group which increases the intercarrier interference. As seen in Fig. 4.1, a degradation of the BER performance from approximately 0.1×10^{-3} to 3×10^{-3} occurs when the frequency offset increases from 0 to 30%. From Fig. 4.2, we can see that, at low SF_{freq}, the MAI is the main factor that causes the performance degradation since there are fewer subcarriers in each group which decreases the effect of the intercarrier interference due to frequency offset than the case with higher SF_{freq}.

Fig. 4.3 shows the BER vs. the normalized frequency offset with respect to the subcarrier spacing for different spreading factors with $E_b/N_o = 20$dB. From Fig. 4.3 it can be observed that at high E_b/N_o, higher SF_{freq} performs better than higher SF_{time} for a fixed SF of 32 when there is no frequency offset since the frequency diversity allows the system to achieve higher absolute performance. However, as the frequency offset increases, higher SF_{time} gives better performance as the effect of the intercarrier interference becomes dominant. From Fig. 4.3, we can also see that, when the frequency offset is higher than 10%, the BER performance starts to deteriorate for the higher SF_{freq}, while the lower SF_{freq} tolerates a frequency offset

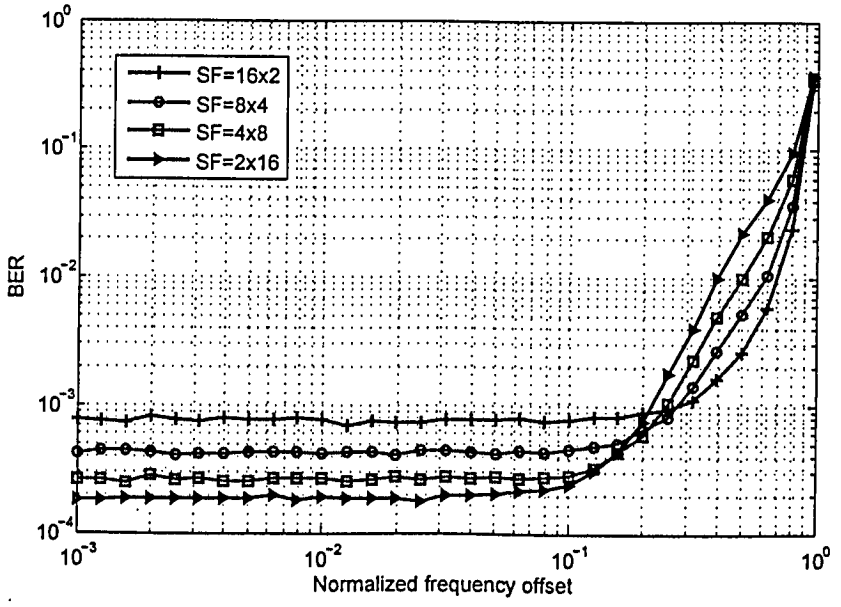

Figure 4.3: BER vs. normalized frequency offset at E_b/N_o = 20dB for different SF.

up to 20% of the frequency spacing between adjacent subcarriers. These results suggest that for a fixed total spreading factor, increasing SF_{time} with respect to SF_{freq} will decrease the sensitivity of the VSF-OFCDM system to the effect of the frequency offset. Therefore, increasing SF_{time} with respect to SF_{freq} for a total fixed SF of 32 will result in an overall better performance of the OFCDM system in the presence of considerable frequency offset.

Figs. 4.4 and 4.5 show the BER vs. E_b/N_o with 128 subcarriers having carrier frequency offsets of 0 and 30% for different number of users with total SF of 2x16 and 16x2 respectively. It can be observed from these figures that as the number of users increases, the degradation in performance increases as well for both spreading factors. This is to be expected since the intercarrier interference terms ICI_2 and ICI_g are proportional to the number of users. From Fig. 4.4, we can see that, for SF=2x16, the effect of increasing the frequency offset from 0 to 30% for 16 users is almost similar to doubling the number of users from 16 users to 32 users in terms of the degradation of the BER performance. From Fig. 4.4, we can also see that, as the number of users increases from 16 to 48 users, the degradation of the BER performance

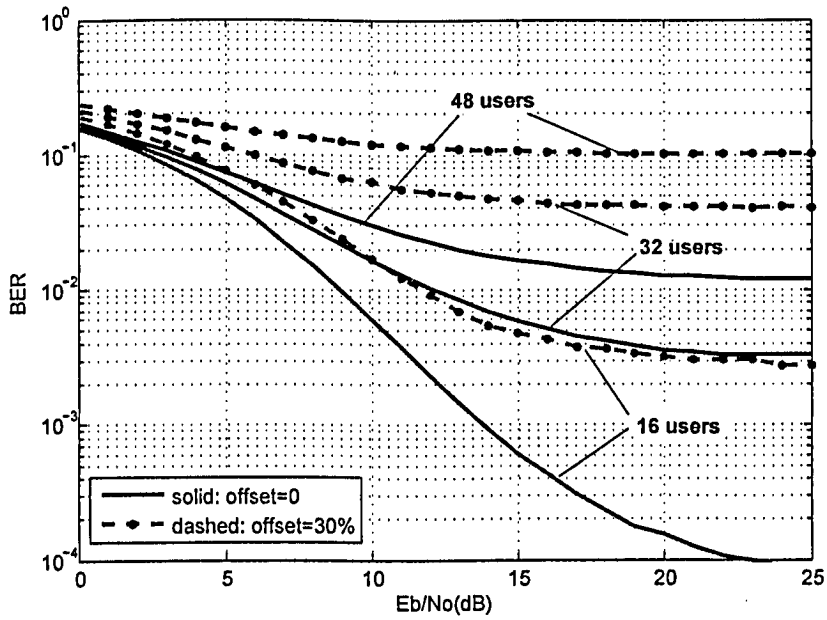

Figure 4.4: BER vs. E_b/N_o with 128 subcarriers and SF=2x16 for different number of users at frequency offsets of 0 and 30%.

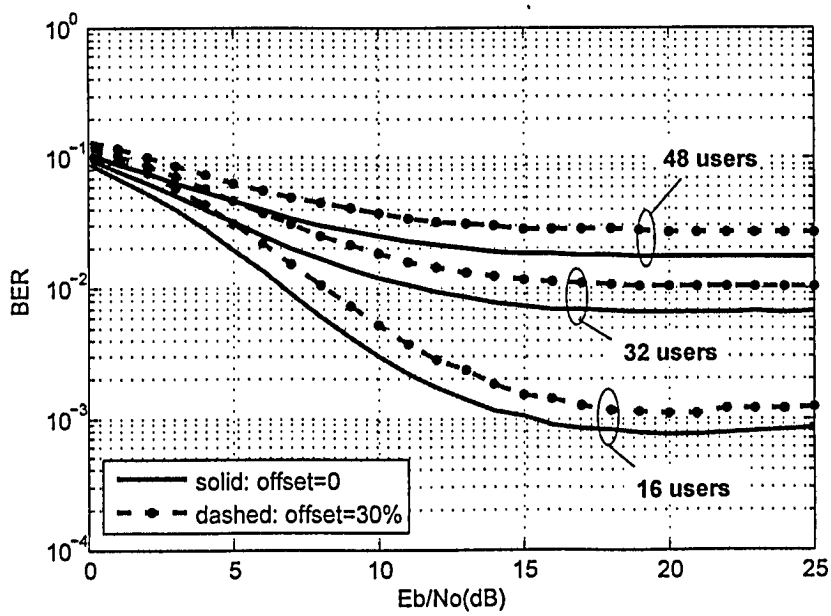

Figure 4.5: BER vs. E_b/N_o with 128 subcarriers and SF=16x2 for different number of users at frequency offsets of 0 and 30%.

due to the increase of frequency offset from 0 to 30% increases from approximately 0.29×10^{-2} to 8.9×10^{-2}. In Fig. 4.5, for SF=16x2, as the number of users increases from 16 to 48 users, the degradation of the BER performance due to the increase of frequency offset from 0 to 30% increases from approximately 0.5×10^{-3} to 10×10^{-3}. From these results, we can see that, the degradation due to increasing the number of users is more pronounced with the higher SF_{freq} since we have more subcarriers in each group as mentioned earlier.

4.2 CFO Estimation and Correction

Due to the adverse impact of frequency offset on VSF-OFCDM systems as seen in the previous section, a reliable estimation of the frequency offset is considered as a basic step in the coherent demodulation process. The carrier frequency offset estimation process can be divided into two fundamental steps which are coarse acquisition and tracking. In this work, we focus on the estimation and correction of the frequency offset in a tracking mode. For OFDM and MC-CDMA systems, similar algorithm have been proposed in [19, 20]. In this work, a CFO correction scheme based on the Maximum Likelihood (ML) estimation principle is proposed for VSF-OFCDM systems using MRC receiver.

4.2.1 Likelihood Function

The log likelihood function considered in our analysis is given by [41]

$$\Lambda = \frac{2}{N_o} \int_{T_o} \mathrm{Re}\{r(t)\tilde{r}^*(t)\} dt, \tag{4.30}$$

where T_o is the observation period and it should satisfy $T_o \geq T_c$.

We can write the received signal in (4.2) as

$$r(t) = \sum_{j} \sum_{g=1}^{G} \sum_{k=1}^{K_g} b_{j,g}^{(k)} \sum_{l=1}^{M} \alpha_{l,g} c_{j,l}^{F(k)} e^{i\left(2\pi(f_{l,g}+f_d)t+\phi_{l,g}\right)} \sum_{n=1}^{N} c_{j,l,n}^{T(k)} p(t-(jN+n)T_c) + n(t), \tag{4.31}$$

$\widetilde{r}(t)$ is the estimate of $r(t)$ and is given by

$$\widetilde{r}(t) = \sum_{j} \sum_{g=1}^{G} \sum_{k=1}^{K_g} b_{j,g}^{(k)} \sum_{l=1}^{M} \alpha_{l,g} c_{j,l}^{F(k)} e^{i\left(2\pi(f_{l,g}+\widetilde{f}_d)t+\phi_{l,g}\right)} \sum_{n=1}^{N} c_{j,l,n}^{T(k)} p(t-(jN+n)T_c), \tag{4.32}$$

where $\widetilde{f}_d$ is the estimate of the offset frequency f_d. A perfect estimation of the fading amplitude and phase is considered for each subcarrier.

Our objective is to maximize this likelihood function based on the ML estimation principle. We will assume in our analysis that the receiver performs the coarse frequency offset correction with training sequences before data transmission and we will consider the frequency offset in the tracking process only.

The log likelihood function depends on the data sequence and the number of subcarriers. The data dependence can be removed by averaging the log likelihood function over all the possible values of the data and fading parameters. In our case, we will define the dependence on data and fading parameters during the n^{th} chip of the j^{th} bit as follows

$$d_{m,g} = \sum_{k=1}^{K_g} \alpha_{m,g} b_{j,g}^{(k)} c_{j,m}^{F(k)} c_{j,m,n}^{T(k)}. \tag{4.33}$$

The received signal can now be written as

$$r(t) = \sum_{g=1}^{G} \sum_{l=1}^{M} d_{l,g} e^{i\left(2\pi(f_{l,g}+f_d)t+\phi_{l,g}\right)}. \tag{4.34}$$

Considering the observation period to be T_c, the log likelihood function becomes

$$\begin{aligned}\Lambda &= \frac{2}{N_o}\int_0^{T_c} \mathrm{Re}\Big\{\sum_{g=1}^{G}\sum_{m=1}^{M} d_{m,g} r(t) e^{-i(2\pi f_{m,g}t+\phi_{m,g})} e^{-i(2\pi \widetilde{f}_d t)}\Big\} dt \\ &= \frac{2}{N_o}\sum_{g=1}^{G}\sum_{m=1}^{M} d_{m,g} \times \mathrm{Re}\{q_{m,g}\},\end{aligned} \tag{4.35}$$

where

$$q_{m,g} = \int_0^{T_c} r(t) e^{-i(2\pi f_{m,g}t+\phi_{m,g})} e^{-i(2\pi \widetilde{f}_d)t} dt, \tag{4.36}$$

which can be re-written as

$$q_{m,g} = \sum_{\acute{g}=1}^{G}\sum_{l=1}^{M}\int_0^{T_c} d_{l,\acute{g}} e^{i\left(2\pi(f_{l,\acute{g}}-f_{m,g}+\Delta f_d)t+\phi_{l,\acute{g}}-\phi_{m,g}\right)} dt, \tag{4.37}$$

where

$$\Delta f_d = f_d - \widetilde{f}_d. \tag{4.38}$$

Therefore, we can write

$$\begin{aligned}Re\{q_{m,g}\} &= \sum_{\acute{g}=1}^{G}\sum_{l=1}^{M}\int_0^{T_c} d_{l,\acute{g}} \cos\left(2\pi(f_{l,\acute{g}} - f_{m,g} + \Delta f_d)t + \phi_{l,\acute{g}} - \phi_{m,g}\right) dt \\ &= \sum_{\acute{g}=1}^{G}\sum_{l=1}^{M} d_{l,\acute{g}} \frac{\sin(2\pi(f_{l,\acute{g}} - f_{m,g} + \Delta f_d)T_c + \phi_{l,\acute{g}} - \phi_{m,g}) - \sin(\phi_{l,\acute{g}} - \phi_{m,g})}{2\pi(f_{l,\acute{g}} - f_{m,g} + \Delta f_d)}.\end{aligned} \tag{4.39}$$

By making some mathematical approximations that are valid for low SNR [15], we obtain the likelihood function for the carrier frequency offset as follows

$$\bar{\Lambda} = \frac{1}{N_o^2}\Big(\sum_{g=1}^{G}\sum_{m=1}^{M} d_{m,g} \times \mathrm{Re}\{q_{m,g}\}\Big)^2. \tag{4.40}$$

We remove the data dependence by averaging the likelihood function over all the values

of the data and fading parameters $d_{m,g}$. After some calculations, we get

$$E[\bar{\Lambda}] = \frac{T_c^2 E[d_{l,\acute{g}}{}^2]}{4\pi^2 N_o^2} \sum_{g=1}^{G} \sum_{m=1}^{M} \sum_{\acute{g}=1}^{G} \sum_{l=1}^{M} \frac{1-\cos(2\pi\Delta f_d T_c)}{((\Delta f_d + f_{l,\acute{g}} - f_{m,g})T_c)^2}, \tag{4.41}$$

where $\Delta f_d T_c$ is the normalized frequency offset error with respect to the subcarrier spacing.

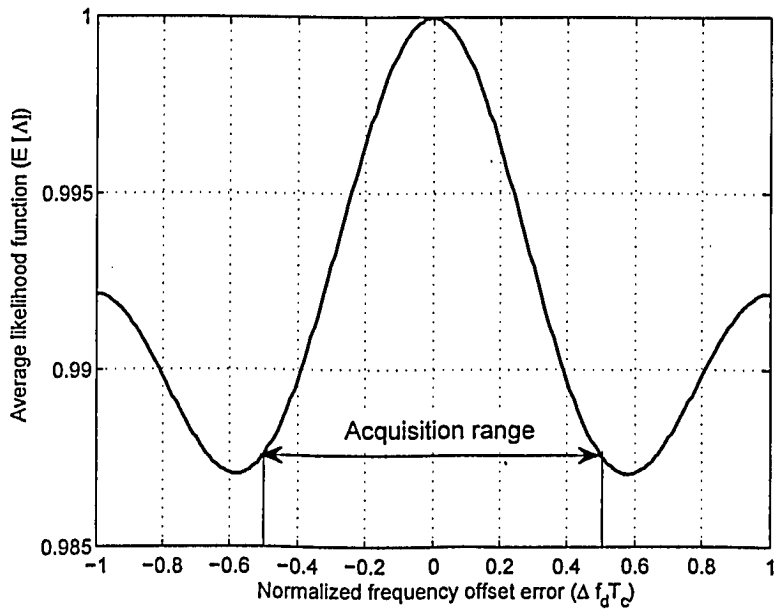

Figure 4.6: Average value of the likelihood function vs. the normalized frequency offset error.

Fig. 4.6 shows the normalized mean value of the likelihood function versus the normalized frequency offset error ($\Delta f_d T_c$) with 128 subcarriers. It can be seen from the figure that the likelihood function reaches a maximum value for $\Delta f_d T_c = 0$ and that the acquisition range is between -0.5 and 0.5 of the subcarrier spacing. The optimum value of $\widetilde{f_d}$ is therefore the one that maximizes the likelihood function. To find the maximum of this function, a non linear algorithm is employed as discussed in the next section.

4.2.2 Correction of CFO

We propose to use the gradient method to maximize the likelihood function. The gradient method is chosen because it is easy to implement and it requires low computational complexity.

Averaging on data and fading parameters and then taking the derivative of the likelihood function in (4.40) with respect to $\widetilde{f}_d$ to obtain the ML estimation, we get

$$\begin{aligned}\frac{\partial\bar{\Lambda}}{\partial\widetilde{f}_d} &= \frac{2C}{N_o^2}\sum_{g=1}^{G}\sum_{m=1}^{M}\mathrm{Re}\{q_{m,g}\}\frac{\partial\mathrm{Re}\{q_{m,g}\}}{\partial\widetilde{f}_d} \\ &= \frac{2C}{N_o^2}\sum_{g=1}^{G}\sum_{m=1}^{M}\mathrm{Re}\{q_{m,g}\}\times p_{m,g},\end{aligned} \tag{4.42}$$

where

$$p_{m,g} = \frac{\partial\mathrm{Re}\{q_{m,g}\}}{\partial\widetilde{f}_d}. \tag{4.43}$$

By differentiating (4.39), we get

$$p_{m,g} = 2\pi\sum_{\acute{g}=1}^{G}\sum_{l=1}^{M}\left[d_{l,\acute{g}}\int_0^{T_c} t\sin\left(2\pi(f_{l,\acute{g}} - f_{m,g} + \Delta f_d)t + \phi_{l,\acute{g}} - \phi_{m,g}\right)dt\right], \tag{4.44}$$

$$\begin{aligned}p_{m,g} = 2\pi\sum_{\acute{g}=1}^{G}\sum_{l=1}^{M}d_{l,\acute{g}}\Bigg[&\frac{[-T_c\cos\left(2\pi\Delta f_d T_c + \phi_{l,\acute{g}} - \phi_{m,g}\right)]}{2\pi(f_{l,\acute{g}} - f_{m,g} + \Delta f_d)} \\ &+ \frac{[\sin(2\pi\Delta f_d T_c + \phi_{l,\acute{g}} - \phi_{m,g}) - \sin(\phi_{l,\acute{g}} - \phi_{m,g})]}{(2\pi(f_{l,\acute{g}} - f_{m,g} + \Delta f_d))^2}\Bigg].\end{aligned} \tag{4.45}$$

For the estimation of the frequency offset, we use the gradient method and hence,

$$\widetilde{f}_{d_{r+1}} = \widetilde{f}_{d_r} + k\epsilon_r, \tag{4.46}$$

where k is a positive constant, $\widetilde{f}_{d_r}$ and $\widetilde{f}_{d_{r+1}}$ are the estimation of f_d at the r^{th} and $(r+1)^{th}$

iteration respectively and ϵ_r is given by the following expression

$$\epsilon_r = \sum_{g=1}^{G} \sum_{m=1}^{M} \mathrm{Re}\{q_{m,g}\} \times p_{m,g}. \tag{4.47}$$

4.2.3 Numerical Results

In this section, we use the same simulation parameters as in section 4.1.2. Fig. 4.7 shows the BER of the VSF-OFCDM system vs. the normalized (with respect to the subcarrier spacing) frequency offset ($f_d T_c$) for different spreading factors ($SF = SF_{time} \times SF_{freq}$) at E_b/N_o = 10dB. This figure shows that for example, for a BER of 10^{-2}, the performance starts to deteriorate at $f_d T_c$=0.1, 0.2, 0.25 and 0.3 for a total SF of 2x16, 4x8, 8x4 and 16x2 respectively. This means that if we can mitigate the frequency offset to less than that level for the different SF_{time} and SF_{freq}, we can improve the system performance significantly.

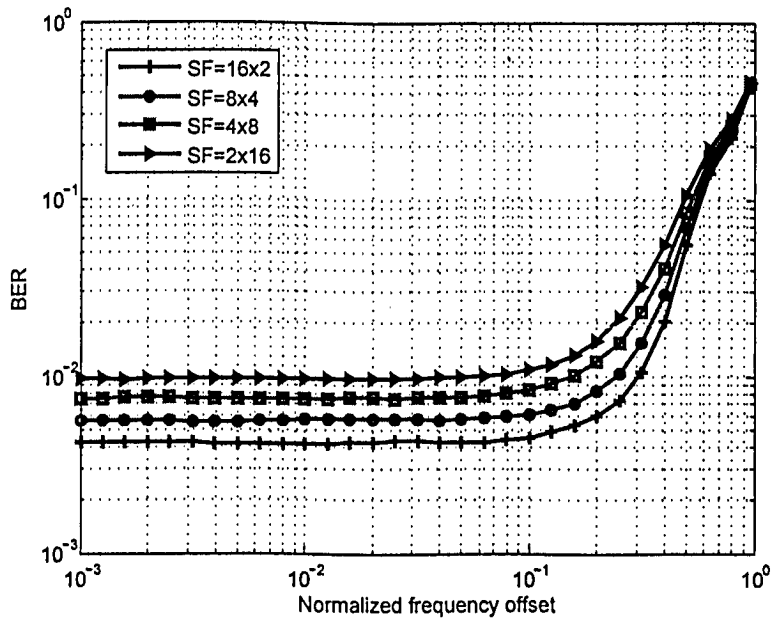

Figure 4.7: BER vs. normalized frequency offset at E_b/N_o = 10dB for different SF.

We first investigate the convergence speed and the sensitivity of the gradient method with different spreading factors with 16 users simultaneously using the channel. In Figs. 4.8 and

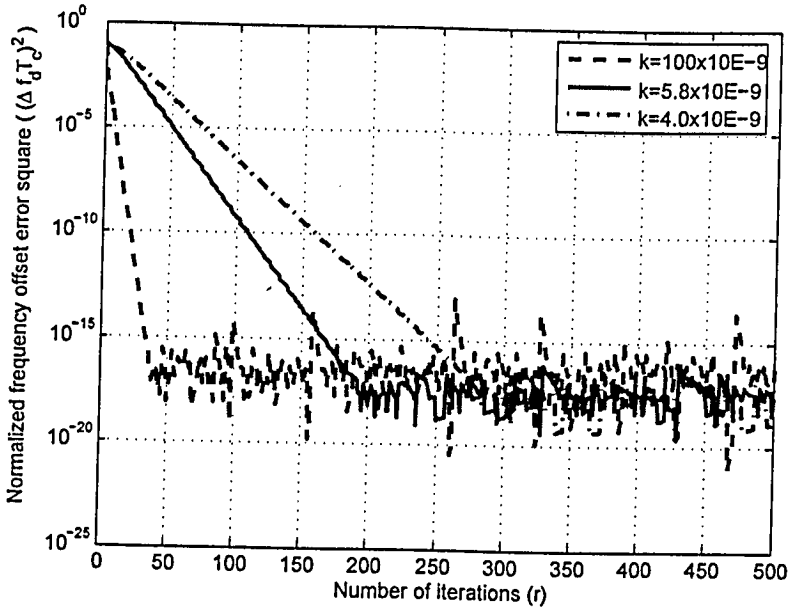

Figure 4.8: CFO correction results vs. number of iterations for different values of k and SF=2x16

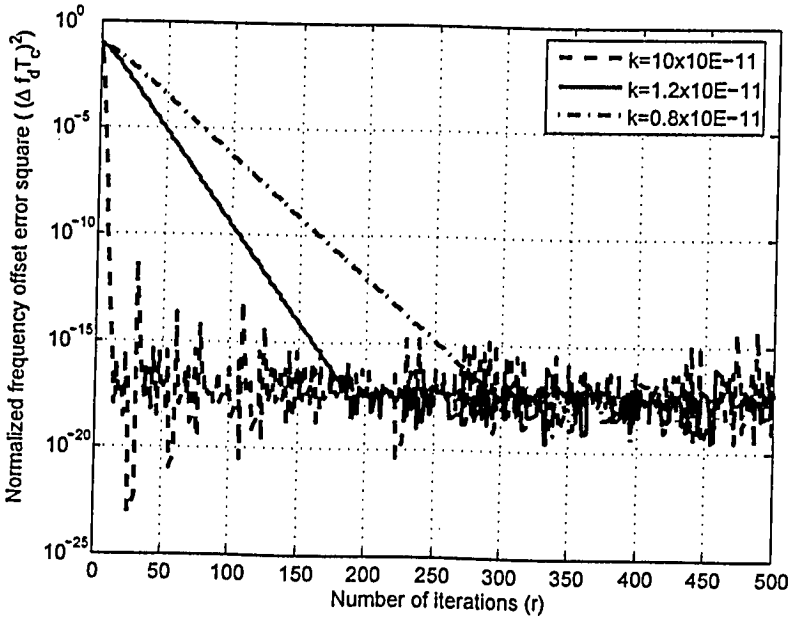

Figure 4.9: CFO correction results vs. number of iterations for different values of k and SF=16x2

4.9, the number of iterations are plotted versus the square of the normalized frequency offset error. In Fig. 4.8, we use a total SF of 2x16 which represents a case with high frequency

domain spreading and we change the constant k to be $k = 100 \times 10^{-9}$, $k = 5.8 \times 10^{-9}$ and $k = 4 \times 10^{-9}$. The same is done in Fig. 4.9 but with a total SF of 16x2 and the constant k takes the values $k = 10 \times 10^{-11}$, $k = 1.2 \times 10^{-11}$ and $k = 0.8 \times 10^{-11}$. From Figs. 4.8 and 4.9, we notice that with different values of the constant k, the algorithm converges to the same floor of the normalized frequency offset error ($\Delta f_d T_c$) which is around 10^{-8} but at different convergence speeds. Also, different constants will result in different error variances after reaching the error floor. This is because different values of k result in different step sizes of converging to the optimal value (when there is no frequency offset) which affects the rapidity of convergence. If the constant is too large, the algorithm will over-adjust the frequency around the correct value. Smaller values of k will result in smaller error variance but the algorithm will require more iterations to converge to the optimal value. Similar figures can be obtained for the different spreading factors for different values of k. From Figs. 4.8 and 4.9, it is clear that different SF in the time and frequency domain will require different step sizes to converge at the same speed.

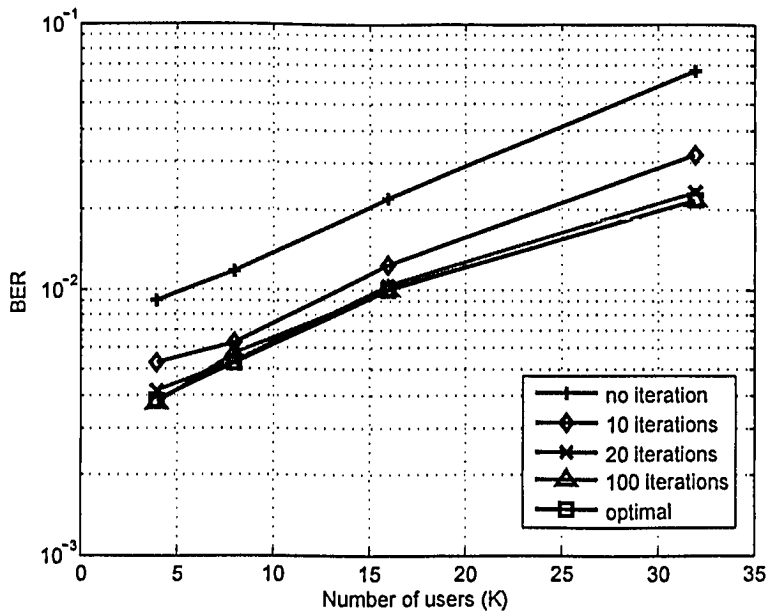

Figure 4.10: BER performance improvement with different number of iterations and SF=2x16

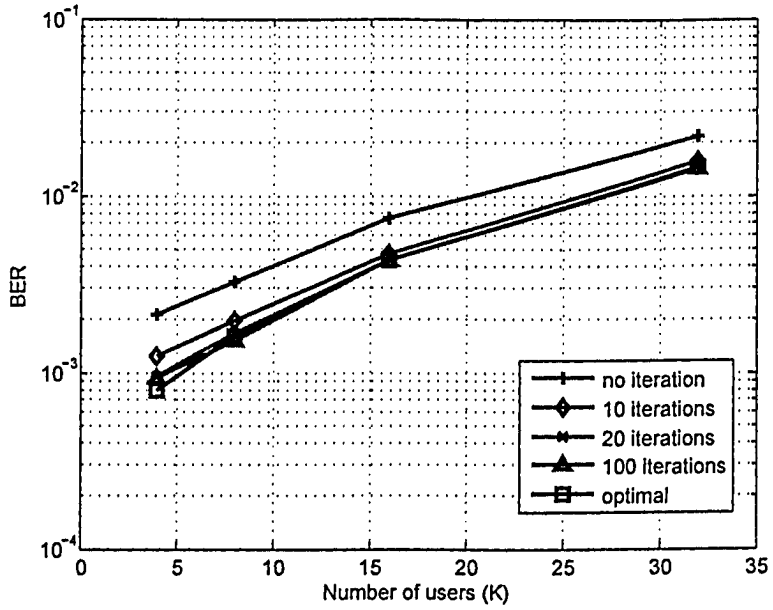

Figure 4.11: BER performance improvement with different number of iterations and SF=16x2

Figs. 4.10 and 4.11 show the BER vs. the number of users with 128 subcarriers and initial normalized frequency offset (with respect to the subcarrier spacing) of 0.3 for different number of iterations with total SF of 2×16 and 16×2 respectively. The BER is calculated using equations (4.21)-(4.28) together with the results of the normalized frequency offset error after a fixed number of iterations obtained from Figs. 4.8 and 4.9, for a total SF of 2x16 and 16x2 respectively. The value of the constant k is appropriately adjusted such that after the same number of iterations, the frequency offsets converge to the same value in all the cases. It was shown in section 4.1.2 that, when the total spreading factor is fixed to 32, the OFCDM system with higher SF_{freq} is more sensitive to frequency offset than that with lower SF_{freq}. This effect can be seen in Figs. 4.10 and 4.11, where lower SF_{freq} converges faster to the optimal value. The figures show that within only 20 iterations, we are close to the optimal value when the normalized frequency offset can be minimized to the case with negligible offset, which significantly improves the BER performance for different number of users and different spreading factors.

Chapter 5

Adaptive Modulation for a VSF-OFCDM System

Adaptive modulation increases the data rates in wireless transmission over fading channels by adapting to the changing channel conditions and making use of spectrally efficient modulation schemes [42] . Adaptive modulation is also a way to improve the tradeoff between spectral efficiency and BER. This is done by exploiting the fading dynamics of the Rayleigh channel. Periods of low fade, or high gain, will improve the instantaneous SNR, allowing higher rate modulation schemes to be employed with low probability of error. Periods of high fade will lower the effective SNR, and therefore low rate modulation should be used to make transmission more robust. Various selection algorithms have been proposed for adaptive systems to decide between modulation schemes based on the channel conditions [43]. In this chapter, we propose an adaptive modulation algorithm for the VSF-OFCDM system with adaptive subcarrier allocation to increase the spectral efficiency without sacrificing the BER performance under different spreading factors assuming there is no CFO. We use a fixed threshold to switch between the modulation levels depending on the estimated SINR of the users in each group. In multicarrier systems, subcarriers are often grouped together and adaptation is performed on the entire subcarrier group to reduce the computational

complexity and signaling overhead [44]. Since the adaptive subcarrier allocation algorithm is implemented on subcarrier groups, it lends itself to group-adaptive modulation. The proposed algorithm provides an increase in spectral efficiency than using BPSK only, without increasing the total transmit power.

5.1 Proposed Adaptive Modulation Algorithm

We propose a threshold-based adaptive modulation algorithm for downlink VSF-OFCDM system that switches between the different modulations levels depending on the estimated SINR for each group. The SINR is estimated at the receiver and is reported to the transmitter through a feedback channel and rate selection is done at the transmitter. The modulation level is selected such that it maintains the BER below a desired performance threshold. To have a constant estimated channel SINR for all the OFCDM symbol durations, we use the same assumption of a slow fading channel, which is necessary to ensure that channel conditions do not change drastically over a symbol duration. In the proposed algorithm, the same power is allocated to each subcarrier under a given total transmit power.

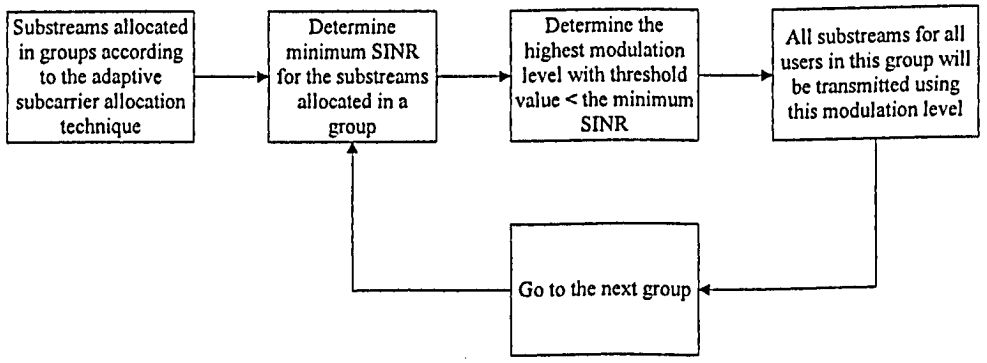

Figure 5.1: Proposed Adaptive Modulation Flowchart.

The flowchart for the proposed algorithm is shown in Fig. 5.1; the steps for the algorithm are as follows:

Step 1: For each group, determine the substream with minimum SINR to ensure that

the level of modulation used will be suitable for transmitting all the substreams in this group.

Step 2: Compare the minimum SINR in each group with the threshold level for different modulation techniques; these thresholds are calculated according to the desired BER.

Step 3: The highest modulation level with a threshold value lower than the minimum SINR calculated for a certain group is chosen and all substreams in this group are transmitted using this modulation level.

5.2 Performance Analysis

In our analysis for using adaptive modulation in VSF-OFCDM systems, we consider two performance metrics: spectral efficiency and BER. The modulation schemes chosen for adaptation in this work are BPSK, QPSK, 8PSK and 16QAM. We consider maximal ratio combining (MRC) receiver to give more weight to subcarriers that experience more favorable fading characteristics as mentioned before. Without loss of generality, if we aim to recover the data transmitted by user 1 in group 1, the SINR ($\gamma_{j,1}^{(1)}$) is calculated from (4.26) by setting $f_d = 0$ since we consider perfect estimation and correction of the frequency offset. Hence, we can write the SINR as

$$\gamma_{j,1}^{(1)} = \frac{2NPT_c \sum_{m=1}^{M} (\alpha_{m,1}^{(1)\,2})}{(K_1 - 1)PT_c E[\alpha_{m,1}^{(k)\,2}] + N_o}. \tag{5.1}$$

The bit error rates using BPSK, QPSK, 8PSK and 16QAM modulations [45] for each user k in group g during the j^{th} transmitted symbol is given by

$$P_{BPSK}(\gamma_{j,g}^{(k)}) = \mathrm{Q}\left(\sqrt{2\gamma_{j,g}^{(k)}}\right), \tag{5.2}$$

$$P_{QPSK}(\gamma_{j,g}^{(k)}) = \mathrm{Q}\left(\sqrt{\gamma_{j,g}^{(k)}}\right), \tag{5.3}$$

$$P_{8PSK}(\gamma_{j,g}^{(k)}) = \frac{2}{3}\mathrm{Q}\left(\sin\frac{\pi}{8}\sqrt{2\gamma_{j,g}^{(k)}}\right), \tag{5.4}$$

$$P_{16QAM}(\gamma_{j,g}^{(k)}) = \frac{3}{4}\mathrm{Q}\left(\sqrt{0.2\gamma_{j,g}^{(k)}}\right). \tag{5.5}$$

To evaluate the mean BER of adaptive modulation $P_{adaptive}(\gamma)$ we use

$$P_{adaptive}(\gamma) = \frac{P_{BPSK}(\gamma)\, N_{BPSK} + P_{QPSK}(\gamma)\, N_{QPSK} + P_{8PSK}(\gamma)\, N_{8PSK} + P_{16QAM}(\gamma)\, N_{16QAM}}{N_{total}}. \tag{5.6}$$

where γ is the SNR, N_{BPSK}, N_{QPSK}, N_{8PSK} and N_{16QAM} are the number of substreams transmitted using BPSK, QPSK, 8PSK and 16QAM respectively and N_{total} is the total number of substreams for all users, $P_{BPSK}(\gamma)$, $P_{QPSK}(\gamma)$, $P_{8PSK}(\gamma)$, $P_{16QAM}(\gamma)$ are the mean bit error rates for BPSK, QPSK, 8PSK and 16QAM respectively calculated from (5.2)- (5.5) by averaging over all users, subcarriers and transmitted symbols.

In order to accommodate a lower target BER without increasing the required SINR, we use Forward Error Correction (FEC) coding. The varieties of FEC codes include Reed-Solomon codes, BCH codes, convolutional codes and turbo codes. We use BCH codes in our analysis. BCH codes [41] constitute an efficient class of linear codes and have the capability of detecting and correcting symbol errors. A BCH (n, k) code is a block code that has a total of n encoded symbols and k original information symbols that is capable of correcting up to $l(< n)$ errors. The corresponding coding rate is $R_c = k/n$. A good approximation of the BER P_b after decoding is given by [37]

$$P_b = \frac{1}{n}\sum_{i=l+1}^{n} i\binom{n}{i}P_e^i(1-P_e)^{n-i}. \tag{5.7}$$

Further approximation of this formula is given by [46]

$$P_b = P_e\mathrm{Q}\left(\frac{l-nP_e}{\sqrt{nP_e}}\right), \tag{5.8}$$

where P_e is the BER calculated from (5.2)-(5.5).

In our system, we define the spectral efficiency to be the average number of bits sent

per modulation symbol; therefore, the spectral efficiency is the expected value of $\log_2 B$ (bits per symbol), where B is the modulation level. In this analysis, we do not take into account whether the transmitted bits are received correctly or not. Because we have set the target BER to a value that we want the system to operate under, the adaptation system will try to achieve this level of performance.

The spectral efficiency η of the uncoded system is calculated as follows:

$$\begin{aligned} \eta &= \frac{n_{BPSK}\, N_{BPSK} + n_{QPSK}\, N_{QPSK} + n_{8PSK}\, N_{8PSK} + n_{16QAM}\, N_{16QAM}}{N_{total}} \\ &= 1 + \frac{N_{QPSK} + 2N_{8PSK} + 3N_{16QAM}}{N_{total}}, \end{aligned} \tag{5.9}$$

where n_{BPSK}, n_{QPSK}, n_{8PSK} and n_{16QAM} are the number of bits per symbol for BPSK, QPSK, 8PSK and 16QAM respectively.

Equation (5.9) shows that using uncoded adaptive modulation with BPSK, QPSK, 8PSK and 16QAM, we can obtain spectral efficiency between 1 and 4 bits per symbol. As the number of substreams using 16QAM increases, the spectral efficiency becomes closer to 4 bits per symbol.

The performance enhancement achieved by using error correcting coding is paid for by a decrease in spectral efficiency by a factor of R_c. Therefore, the spectral efficiency η_{coded} of the encoded system is calculated by:

$$\begin{aligned} \eta_{coded} &= \eta R_c \\ &= \left(1 + \frac{N_{QPSK} + 2N_{8PSK} + 3N_{16QAM}}{N_{total}}\right) R_c. \end{aligned} \tag{5.10}$$

Equation (5.10) shows that using coded modulation, the spectral efficiency obtained will depend on the coding gain used.

5.3 Numerical Results

As mentioned earlier, modulation is adapted on the basis of the estimated SINR for the sub-streams in each group. The switching levels for using QPSK, 8PSK and 16QAM correspond to the SINR at which the target BER is achieved. Below these threshold levels, BPSK is used. The threshold for activating a given modulation mode can be calculated using the BER expression. For a target BER of 10^{-2}, the thresholds were obtained using (5.2)-(5.5). To accommodate a target BER of 10^{-3}, without increasing the SINR required to achieve this BER, coding is used. We use BCH $(511, 385)$ code corresponding to a coding rate R_c=3/4 which is capable of correcting up to 14 errors. The threshold values for the encoded case were calculated using (5.8). Table 5.1 shows the threshold values for the different modulation schemes.

Table 5.1: Threshold values for different modulation schemes.

Modulation	$BER_{target}=10^{-2}$	$BER_{target}=10^{-3}$, R_c= 3/4
	SINR(dB)	SINR(dB)
QPSK	7.334	6.435
8PSK	12.064	11.033
16QAM	14.860	14.064

In this analysis, we use Monte-Carlo simulation with 1000 runs to compare the BER performance of OFCDM with adaptive subcarrier allocation using BPSK, QPSK, 8PSK, 16QAM and the proposed adaptive modulation technique under different spreading factors. The carrier frequency, f_c, is 5 GHz and the downlink channel bandwidth is 100 MHz. There are 256 subcarriers and we use the same assumption as in section 4.1.2 that each subcarrier experiences frequency non-selective fading and that fading is uncorrelated between subcarriers in the same group as a result of the subcarrier grouping strategy used. We assume no carrier frequency offset between the transmitter and the receiver. We investigate the BER performance for the uncoded case with a target BER of 10^{-2} and the encoded case with a

target BER of 10^{-3} and coding rate R_c=3/4. In this simulation, we evaluate the performance under different SF_{time} and SF_{freq} but with a total fixed SF=32 to provide a suitable performance comparison. We evaluate the performance with 16 users simultaneously assigned to the channel and N substreams transmitted simultaneously for each user to make the data rate identical in each analysis.

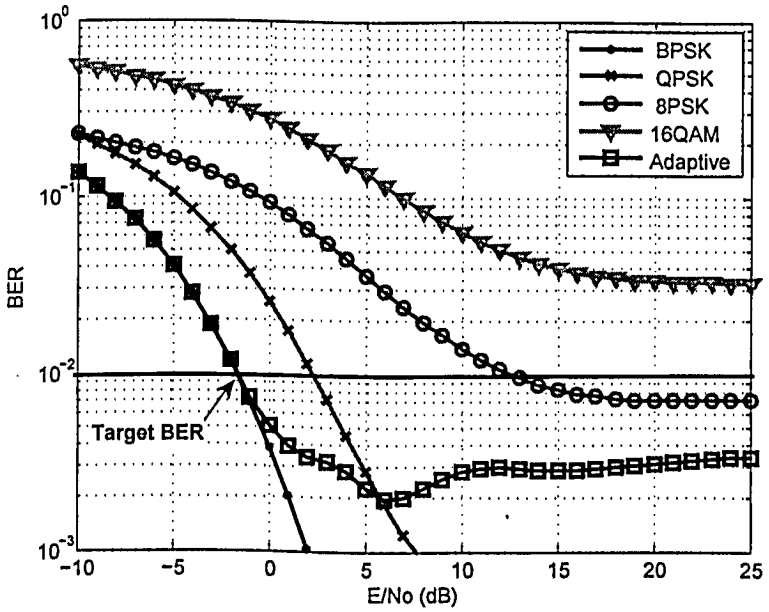

Figure 5.2: BER vs. E/No with 256 subcarriers and SF=16x2 with BER_{target}=10^{-2}

In Figs. 5.2 and 5.3, we plot the BER vs. E/N_o, where E denotes the symbol energy, for BPSK, QPSK, 8PSK, 16QAM and using the proposed adaptive modulation with spreading factors of 16x2 and 2x16 respectively. The results show that at high E/N_o, we can obtain a BER of approximately 3.5x10^{-3} and 2.5x10^{-3} with SF of 16x2 and 2x16 respectively. These results indicate that adaptive modulation improves the BER performance beyond what 8PSK and 16QAM can provide. This improvement allows the system to experience higher spectral efficiency than BPSK while achieving a better BER performance than 8PSK and 16QAM. An increase in the BER with adaptive modulation than the case of BPSK and QPSK at higher E/N_o is expected since no non-adaptive scheme provides better performance while simultaneously providing better spectral efficiency. From Figs. 5.2 and 5.3, we also

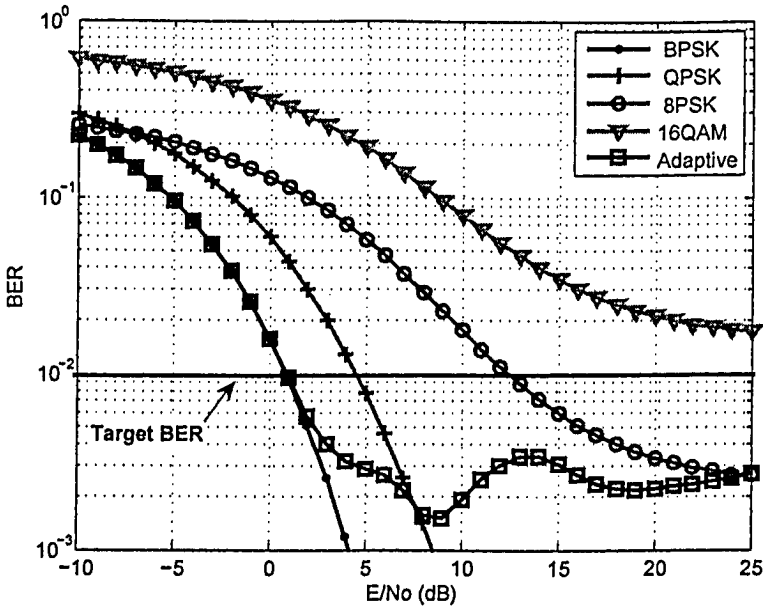

Figure 5.3: BER vs. E/No with 256 subcarriers and SF=2x16 withBER_{target}=10^{-2}

notice that the performance of adaptive modulation begins by overlapping the BPSK curve as BPSK is the primary modulation scheme used at low E/N_o. At high E/N_o, the curves for 8PSK, 16QAM and adaptive modulation hit a performance floor. This performance floor is due to the interference experienced by the system at high E/N_o. It can also be seen from the figures that the adaptive system BER is better than the target BER, resulting in measured mean bit error rates lower than the target except for very low values of E/N_o (noise-limited region). This can be explained by the group-adaptation regime which was based on the principle of using the lowest SINR in each group for modulation level estimation, leading to a pessimistic estimate for the entire group. This is necessary to guarantee that each user has a BER better than the target.

Similar results are obtained when a coding rate R_c= 3/4 is used with a target BER of 10^{-3} for different spreading factors. Figs. 5.4 and 5.5 show the BER vs. E/N_o for the proposed adaptive modulation with different spreading factors for the uncoded and encoded case respectively.

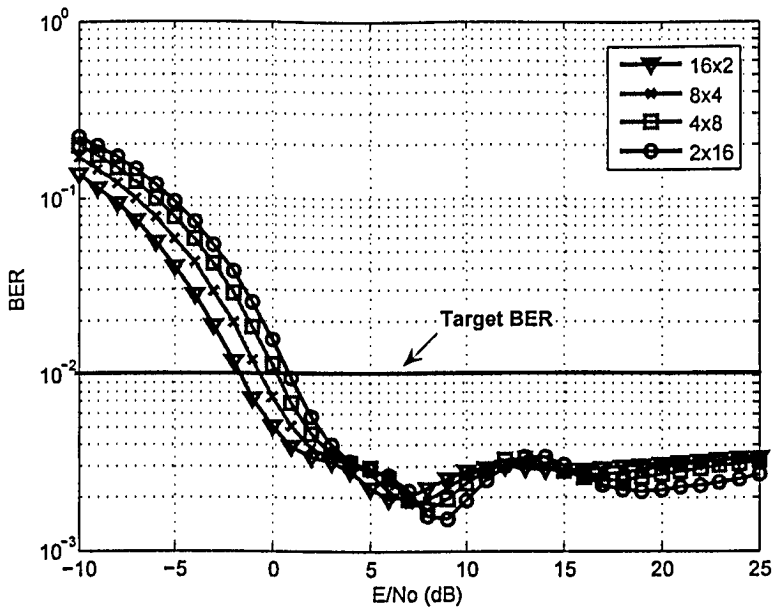

Figure 5.4: BER comparison curves for uncoded adaptive modulation with different SF for BER_{target}=10^{-2}

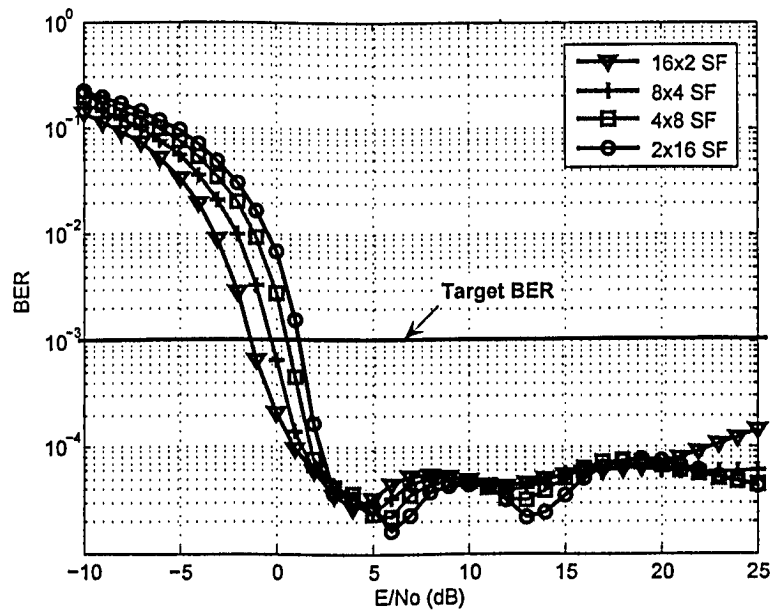

Figure 5.5: BER comparison curves for encoded adaptive modulation with different SF for BER_{target}=10^{-3} and R_c=3/4

Fig. 5.4 shows the BER vs. E/N_o for the proposed adaptive modulation with different spreading factors for the uncoded case. We notice that at low E/N_o, when the total SF is fixed, we obtain better BER performance when a higher SF_{time} is used compared to SF_{freq}. This is because more groups are available with the higher SF_{time} and in the noise-limited region, the subcarrier allocation technique is able to assign the substreams to the most favorable groups while the less favorable groups remain unused. The opposite result occurs at high E/N_o where a higher SF_{freq} provides better BER performance. This is because the system performance is limited by MAI; therefore, the adaptive subcarrier allocation technique gives less performance improvement with the higher SF_{time} since the substreams will have to be assigned to the less favorable groups. In this case the higher SF_{freq} gives a better overall performance due to the frequency diversity gained by the system. Similar results are obtained when a coding rate R_c= 3/4 is used with a target BER of 10^{-3} as shown in Fig. 5.5.

The spectral efficiency can be determined by the number of substreams that uses each modulation scheme. Tables 5.2 and 5.3 show the percentage of substreams using each modulation scheme for different values of E/N_o for the uncoded and encoded case respectively.

Table 5.2: Percentage of substreams using different modulations for BER_{target}=10^{-2}

E/N_O(dB)	16x2 SF				2x16 SF			
	BPSK	QPSK	8PSK	16QAM	BPSK	QPSK	8PSK	16QAM
-5	100%	0	0	0	100%	0	0	0
5	4%	94%	2%	0	20%	80%	0	0
15	2%	22%	58%	18%	0	16%	79%	5%
25	2%	17%	39%	42%	0	11%	60%	29%

From Tables 5.2 and 5.3, we notice that at low E/N_o, most of the substreams use BPSK modulation. As E/N_o increases, the number of substreams using higher order modulation increases until 16QAM becomes the modulation scheme used more often and BPSK is rarely

Table 5.3: Percentage of substreams using different modulations for BER_{target}=10^{-3} and $R_c = 3/4$

E/N_O(dB)	16x2 SF				2x16 SF			
	BPSK	QPSK	8PSK	16QAM	BPSK	QPSK	8PSK	16QAM
-5	100%	0	0	0	100%	0	0	0
5	1.5%	87%	11.5%	0	3%	97%	0	0
15	1%	14%	47%	38%	0	11%	77%	12%
25	1%	11%	26%	62%	0	6%	16%	78%

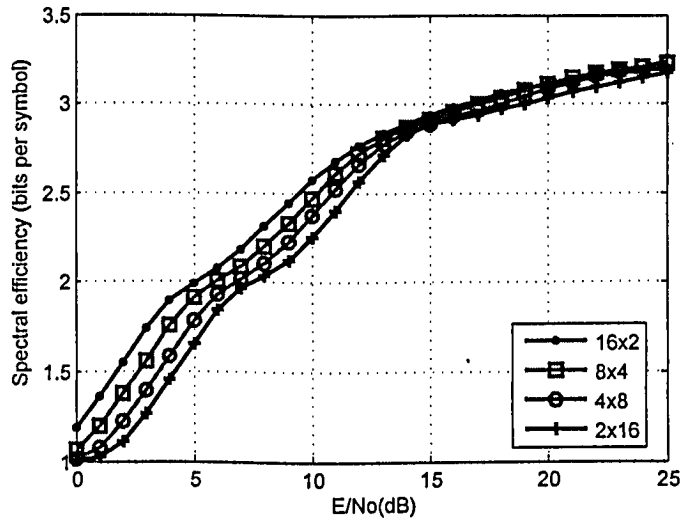

Figure 5.6: Spectral efficiency for uncoded adaptive modulation with different SF for BER_{target}=10^{-2}

used. We also notice that as E/N_o increases, more substreams use higher order modulation when using higher SF_{time} compared to SF_{freq}. This is because for higher SF_{time}, there are more available subcarrier groups which provide a better chance of locating subcarriers with the best fading characteristics. This results in minimizing MAI and maximizing the average SINR, thus more substreams pass the threshold for using higher order modulation. As E/N_o increases further, the higher SF_{freq} increases the percentage of substreams using higher order modulation since in the interference-limited region, higher SF_{freq} gives better performance due to the frequency diversity gained by transmitting over several subcarriers experiencing

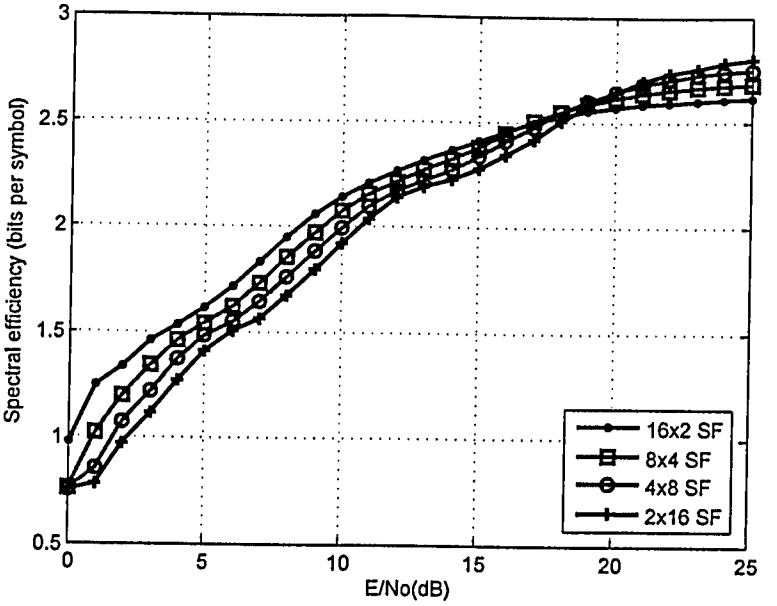

Figure 5.7: Spectral efficiency for encoded adaptive modulation with different SF for BER_{target}=10^{-3} and R_c=3/4

independent fading.

In Figs. 5.6 and 5.7, we plot the spectral efficiency (bits per symbol) vs. E/N_o for the uncoded and encoded case with different spreading factors using the proposed adaptive modulation algorithm according to (5.9) and (5.10) respectively. We notice that as E/N_o increases, the spectral efficiency improves steadily as the system is able to choose more efficient modulation schemes. The results show that at high E/N_o, we can obtain a spectral efficiency up to 3.2 and 2.8 bits per symbol for the uncoded and encoded case respectively. Also, we notice that at low E/N_o, the spectral efficiency increases with higher SF_{time} since more groups are available which maximizes SINR as mentioned earlier. As E/N_o increases, the OFCDM system makes a transition from being noise-limited to being interference-limited and thus the higher SF_{freq} gives better spectral efficiency. This can be seen in Fig. 5.7 when E/N_o exceeds 18 dB.

In Figs. 5.8 and 5.9, we compare the spectral efficiency gained by using uncoded adaptive modulation in OFCDM systems when the adaptive subcarrier allocation technique [14] was

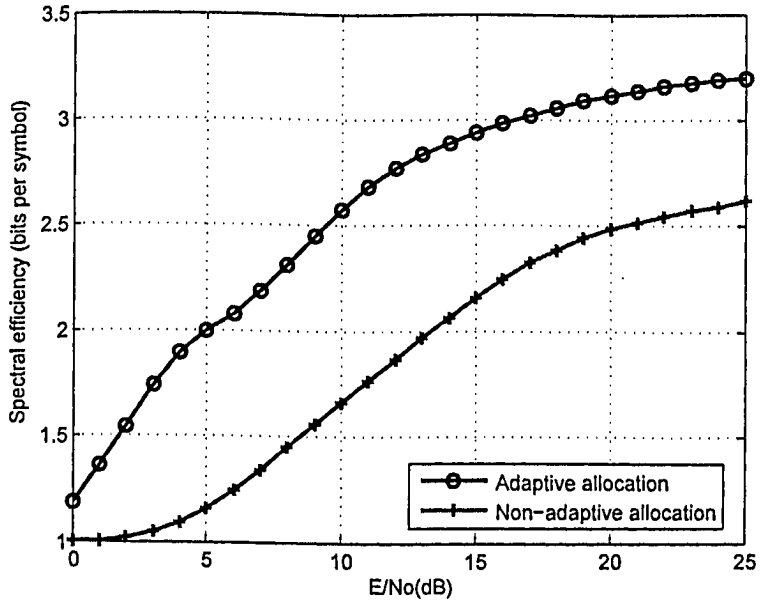

Figure 5.8: Comparison curves of the spectral efficiency of uncoded adaptive modulation with adaptive and non-adaptive allocation for SF=16x2.

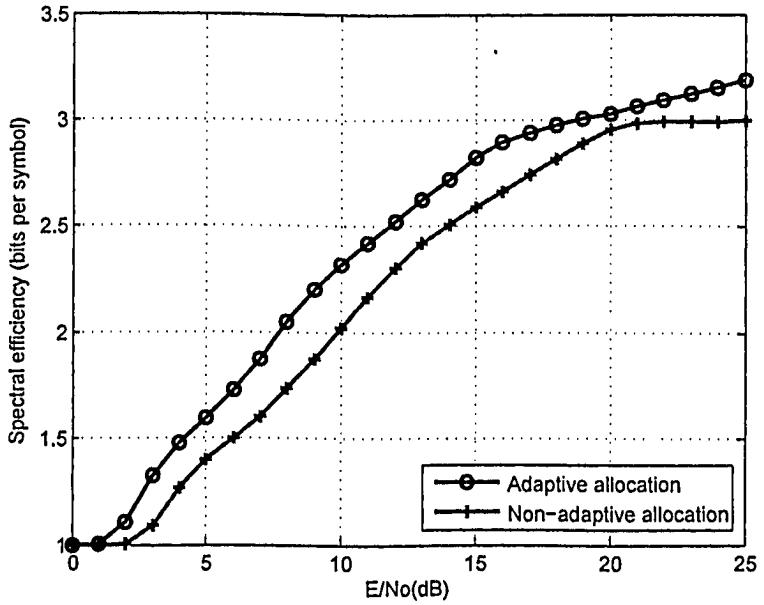

Figure 5.9: Comparison curves of the spectral efficiency of uncoded adaptive modulation with adaptive and non-adaptive allocation for SF=2x16.

used as opposed to using non-adaptive allocation (with adjacent subcarriers) [34] with 16x2 and 2x16 spreading factors respectively. As seen in Fig. 5.8, the spectral efficiency increased from 2.6 to 3.2 bits per symbol for E/N_o= 25 dB when using adaptive modulation in the OFCDM system combined with adaptive subcarrier allocation for SF of 16x2. From Fig. 5.9, we notice less increase in the spectral efficiency with SF of 2x16 compared to SF of 16x2. This is because for a fixed total SF, the subcarrier allocation technique is more effective with higher SF_{time} compared to SF_{freq} as more groups of subcarriers are available to maximize the average SINR. Also, for higher SF_{freq}, the frequency diversity gained by the system improves the signal power with respect to the noise while the subcarrier allocation technique increases the interference power proportional to the signal power which makes the subcarrier allocation technique less effective at higher SF_{freq} [14]. Similar results are obtained for the increase in spectral efficiency with the adaptive subcarrier allocation technique when coding with a rate of 3/4 is used with adaptive modulation in the VSF-OFCDM system for different spreading factors as shown in Figs. 5.10 and 5.11.

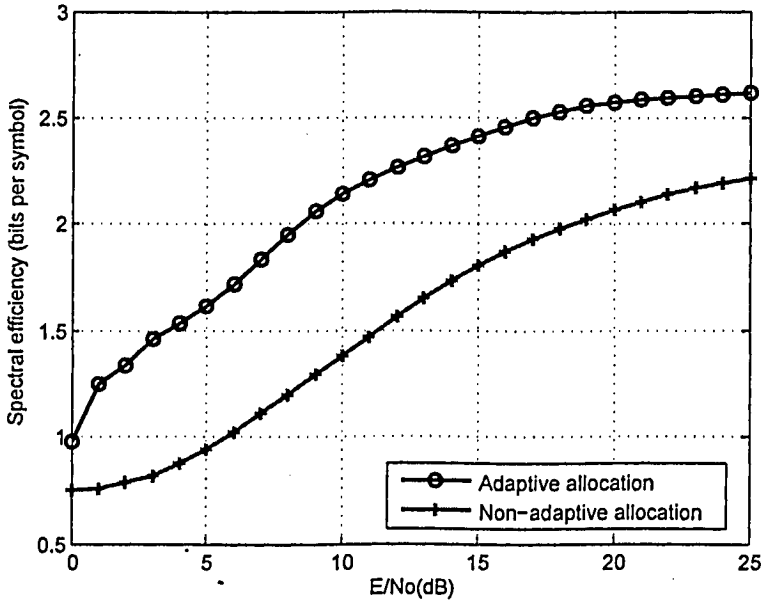

Figure 5.10: Comparison curves of the spectral efficiency of encoded adaptive modulation with adaptive and non-adaptive allocation for SF=16x2 and R_c=3/4.

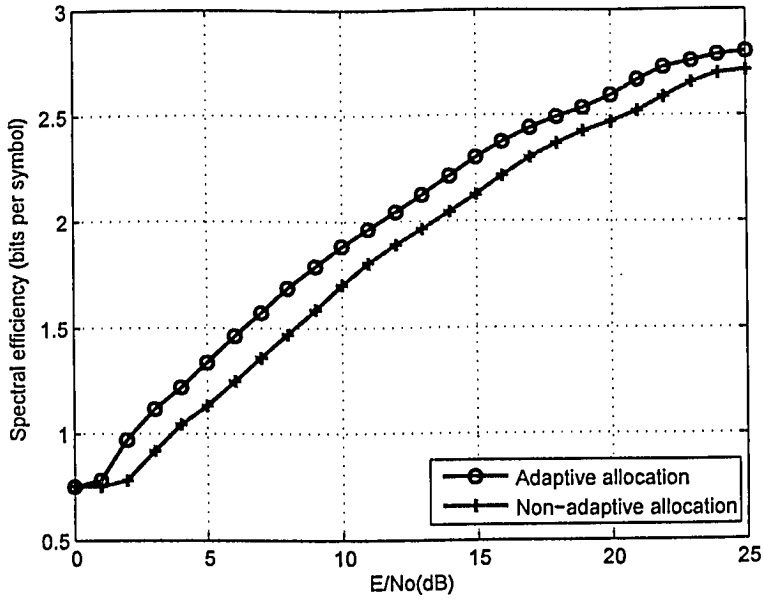

Figure 5.11: Comparison curves of the spectral efficiency of encoded adaptive modulation with adaptive and non-adaptive allocation for SF=2x16 and R_c=3/4.

Although using only higher order modulation can provide more increase in spectral efficiency than adaptive modulation, it degrades the BER performance by increasing the BER above the target values. This means that adaptive modulation provides a good tradeoff between spectral efficiency and BER.

Chapter 6

Conclusions and Future work

6.1 Conclusions

The 4G system can be thought of as an integrated wireless system that enables seamless roaming between technologies. 4G is expected to support the next generation of mobile services as well as the fixed wireless networks. It is intended to provide high data rates, high capacity and low cost services. OFDM and the variations thereof, MC-CDMA and VSF-OFCDM are predicted to be the most applicable multiple access techniques for 4G implementation. In this thesis, we focused on VSF-OFCDM systems which employ two dimensional spreading where the spreading factors can be adaptively changed according to the cell configuration, channel load and propagation channel conditions. VSF-OFCDM can achieve the high capacity and high data rates that are expected from the 4G systems.

VSF-OFCDM systems, like other multicarrier systems, suffer from performance degradation due to carrier frequency offset. In this thesis, the BER performance of downlink VSF-OFCDM using BPSK modulation was analyzed in the presence of carrier frequency offset. From the numerical results, we conclude that, when the total spreading factor was fixed to 32, the VSF-OFCDM system with higher SF_{freq} is more sensitive to frequency offset than that with lower SF_{freq}. Also, the effect of the normalized frequency offset on BER

performance is smaller when the normalized frequency offset is less than 0.1 for the higher SF_{freq} and less than 0.2 for the lower SF_{freq}. In addition, our results show that the degree of degradation due to CFO in the VSF-OFCDM system is also a function of the number of users.

In this thesis, we showed that the BER performance of VSF-OFCDM can be improved significantly when the effect of frequency offset is mitigated. We presented a maximum likelihood estimation of the CFO in a VSF-OFCDM system for the case of low SNR. The results show that the likelihood function reaches a maximum value when the normalized frequency offset is zero. Using the characteristics of the likelihood function and the ML principle, a gradient algorithm was used to minimize the frequency offset for different spreading factors. The numerical results show that our approach is able to estimate and correct the frequency offset with a normalized residual error of less than 10^{-8} for different spreading factors. Different spreading factors in time and frequency domain require different step sizes to converge at the same speed. The results also show that the BER of the VSF-OFCDM system can be improved significantly for different spreading factors after only a few number of iterations.

The need for higher data rates makes it essential to investigate methods to achieve better spectral efficiency. Since adaptive modulation provides more efficient use of the spectrum than the fixed modulation, we proposed an adaptive modulation algorithm for VSF-OFCDM to achieve higher spectral efficiency for a given target BER. The adaptive modulation algorithm was performed on groups of subcarriers and fixed threshold levels were used to switch between the different modulation levels depending on the estimated SINR for each group. The performance of adaptive modulation for a target BER of 10^{-2} was investigated. Coding rate of 3/4 was used for a lower target BER of 10^{-3}. The proposed algorithm provides a spectral efficiency up to 3.2 and 2.8 bits per symbol for a target BER of 10^{-2} for the uncoded case and 10^{-3} for the encoded case respectively without increasing the total transmit power. Our results show that higher spectral efficiency is obtained when adaptive modulation is used with adaptive subcarrier allocation than with non-adaptive allocation for different spread-

ing factors. However, better results were obtained for the spectral efficiency when a higher SF_{time} was used compared to SF_{freq}, as the subcarrier allocation technique is more effective with higher SF_{time}.

6.2 Future work

Based on this work, the following are open areas and potential research directions that might be interesting to pursue in the future

- We estimated the carrier frequency offset in a tracking mode with a small acquisition range due to the particular form of the likelihood function for a multicarrier system. It is worthy to investigate other techniques that can be used to increase the acquisition range.

- We assumed downlink transmission in our analysis. This work can be extended to study the impact of frequency offset for the case of uplink transmission.

- We assumed uncorrelated subcarriers within each group. The effect of non-zero subcarriers correlations within a group would also be of interest.

- We assumed constant transmit power when using adaptive modulation. Another possibility is to study adaptive modulation that uses variable transmit power levels.

- Combining adaptive modulation with adaptive coding is another possible area of investigation.

- We used fixed threshold to switch between the different modulation levels. It would be interesting to investigate methods of adaptively changing the switching levels to further optimize the performance.

Bibliography

[1] K. R. Santhi, V. K. Srivastava, G. SenthilKumaran, and A. Butare., "Goals Of True Broad bands Wireless Next Wave (4G-5G)," in *IEEE Vehicular Technology Conference*, vol. 4, pp. 2317–2321, October 2003.

[2] S. Y. Hui and K. H. Yeung, "Challenges in the Migration to 4G Mobile Systems," *IEEE Communications Magazine*, vol. 41, pp. 54–59, December 2003.

[3] T. Miki, T. Ohya, H. Yoshino, and N. Umeda, "The Overview of the 4th Generation Mobile Communication System," in *International Conference on Information, Communications and Signal Processing*, pp. 1551–1555, December 2005.

[4] K. Tachikawa, "A Perspective on the Evolution of Mobile Communications," *IEEE Communications Magazine*, vol. 41, pp. 66–73, October 2003.

[5] V. DaSilva and E. S. Sousa, "Performance of Orthogonal CDMA Codes for Quasi-Synchronous Communication Systems," in *IEEE International Conference on Universal Personal Communications*, vol. 2, pp. 995–999, October 1993.

[6] N. Yee, J. Linnartz, and G. Fettweis, "Multicarrier CDMA in Indoor Wireless Radio Networks," in *IEEE International Symposium on Personal, Indoor and Mobile Radio Communications*, vol. 3, pp. 109–113, September 1993.

[7] K. Fazel and S. Kaiser, *Multi-carrier Spread Spectrum and Related Topics.* Kluwer Academic Publishers, Boston, USA, 1999.

[8] L. Xiao and Q. Liang, "A Novel MC-2D-CDMA Communication System and Its Detection Methods," in *IEEE International Conference on Communications*, vol. 3, pp. 1223–1227, June 2000.

[9] H. Atarashi, S. Abeta, and M. Sawahashi, "Variable Spreading Factor Orthogonal Frequency and Code Division Multiplexing (VSF-OFCDM) for Broadband Packet Wireless Access," *IEICE Transactions on Communications*, vol. E86-B, pp. 291–299, January 2003.

[10] N. Maeda, Y. Kishiyama, H. Atarashi, and M. Sawashashi, "Variable Spreading Factor-OFCDM with Two Dimensional Spreading that Prioritizes Time Domain Spreading for Forward Link Broadband Wireless Access," in *IEEE Vehicular Technology Conference*, vol. 1, pp. 127–132, April 2003.

[11] A. Matsumoto, K. Miyoshi, M. Uesugi, and O. Kato, "A Study on Time Domain Spreading for OFCDM," in *IEEE International Symposium on Wireless Personal Multimedia Communications*, vol. 2, pp. 725–728, October 2002.

[12] H. Long and Y. H. Chew, "An Adaptive Subcarrier Allocation Scheme for MC-DS-CDMA Systems in the Presence of Multiple Access Interference," in *IEEE International Conference on Communications*, vol. 5, pp. 2894–2898, June 2004.

[13] J. Kim, C. N. Georghiades, and G. M. Huang, "Adaptive Data Transmission Based on Band-Selection for MC-CDMA," in *IEEE Global Telecommunications Conference*, vol. 5, pp. 3125–3129, November 2001.

[14] R. Caldwell and A. Anpalagan, "Performance Analysis of Subcarrier Allocation in Two Dimensionally Spread OFCDM Systems," in *IEEE Vehicular Technology Conference*, September 2006.

[15] Y. Kim, S. Choi, C. You, and D. Hong, "Effect of Carrier Frequency Offset on the Performance of an MC-CDMA System and its Countermeasure Using Pulse Shaping," in *IEEE International Conference on Communications*, vol. 1, pp. 167–171, June 1999.

[16] W. Yang, J. Liu, and S.-X. Cheng, "Effect of Carrier-Frequency Offset on the Performance of Group-Orthogonal Multicarrier CDMA Systems," *Elsevier Signal Processing*, vol. 86, pp. 3934–3940, December 2006.

[17] H. Steendam and M. Moeneclaey, "The Effect of Carrier Frequency Offsets on Downlink and Uplink MC-DS-CDMA," *IEEE Journal on Selected Areas in Communications*, vol. 19, pp. 2528–2536, December 2001.

[18] T. Pollet, "BER Sensitivity of OFDM Systems to Carrier Frequency Offset and Wiener Phase Noise," *IEEE Transactions on Communications*, vol. 43, pp. 191–193, Febraury 1995.

[19] F. Daffara and A. Chouly, "Maximum Likelihood Frequency Detectors for Orthogonal Multicarrier Systems," in *IEEE International Conference on Communications*, vol. 2, pp. 766–771, May 1993.

[20] M. Guainazzo, M. Gandetto, C. Sacchi, and C. S. Regazzoni, "Maximum Likelihood Estimation of Carrier Offset in a Variable Bit Rate Orthogonal Multicarrier CDMA," in *IEEE International Symposium on Image and Signal Processing and Analysis*, vol. 2, pp. 1181– 1185, September 2003.

[21] L. Hanzo, M. Munster, B. J. Choi, and T. Keller, *OFDM and MC-CDMA for Broadband Multi-User Communications, WLANs and Broadcasting.* John Wiley and Sons Ltd., West Sussex, England, 2003.

[22] L. Khalid and A. Anpalagan, "Effect of Frequency Offset on the BER Performance of Variable Spreading Factor OFCDM Systems," in *review, IEEE International Conference on Communications*, 2008.

[23] L. Khalid and A. Anpalagan, "Maximum Likelihood Estimation of Frequency Offset in Variable Spreading Factor OFCDM Systems," in *review, IEEE Global Communications Conference*, 2008.

[24] L. Khalid and A. Anpalagan, "Threshold-Based Adaptive Modulation with Adaptive Subcarrier Allocation in OFCDM-Based 4G Wireless Systems," in *IEEE Vehicular Technology Conference*, September 2006.

[25] L. Khalid and A. Anpalagan, "Performance Analysis of a Threshold-based Group-adaptive Modulation Scheme with Adaptive Subcarrier Allocation in OFCDM Systems," *in review, IEEE Transactions on Wireless Communications*, Revised December 2007.

[26] C. J. Jakes, *Microwave Mobile Communications.* IEEE Press, New Jersy, 1994.

[27] H. Schulze and C. Luders, *Theory and Applications of OFDM and CDMA.* John Wiley and Sons, 2005.

[28] R. Nee and R. Prasad, *OFDM for Wireless Multimedia Communications.* Artech House Publishers, 2000.

[29] S. B. Weinstein and P. M. Ebert, "Data Transmission by Frequency Division Multiplexing Using the Discrete Fourier Transform," *IEEE Transactions on Communications*, vol. 19, pp. 628–634, October 1971.

[30] S. Kaiser, "On the Performance of Different Detection Techniques for OFDM-CDMA in Fading Channels," in *IEEE International Conference on Communications*, vol. 3, pp. 2059 –2063, June 1995.

[31] R. Prasad and S. Hara, "Overview of Multicarrier CDMA," *IEEE Communications Magazine*, pp. 126–133, December 1977.

[32] A. Persson, T. Ottosson, and E. Strom, "Time-Frequency Localized CDMA for Downlink Multi-carrier Systems," in *IEEE International Symposium on Spread Spectrum Techniques and Applications*, vol. 1, pp. 118–122, September 2002.

[33] A. Chouly, A. Brajal, and S. Jourdan, "Orthogonal Muticarrier Techniques Applied to Direct Sequence Spread Spectrum CDMA Systems," in *IEEE Global Telecommunications Conference*, vol. 3, pp. 1723–1728, November 1993.

[34] C. W. You and D. S. Hong, "Multicarrier CDMA Systems Using Time-Domain and Frequency-Domain Spreading Codes," *IEEE Transactions on Communications*, vol. 51, pp. 17–21, January 2003.

[35] N. Maeda, H. Atarashi, and M. Sawahashi, "Performance Comparison of Channel Interleaving Methods in Frequency Domain for VSF-OFCDM Broadband Wireless Access in Forward Link," *IEICE Transactions on Communications*, vol. E86-B, pp. 300–313, January 2003.

[36] H. Xia, H. Bertoni, L. Maciel, A. Stewart, and R. Rowe, " Radio Propagation Characteristics for Line-of-Sight Microcellular and Personal Communications," *IEEE Transactions on Antennas and Propagation*, vol. 41, pp. 1439–1447, October 1993.

[37] T. S. Rappaport, *Wireless Communications: Principles and Practice.* Prentice Hall, Inc.,New York, second ed., 2002.

[38] J.-H. Moon, Y. You, W.-G. Jeon, and J.-H. Paik, "BER Performance of Multiple-Antenna OFCDM With Imperfections," *IEEE Communications Letters*, vol. 8, pp. 12–14, January 2004.

[39] M. Pursley, "Performance Evaluation for Phase Coded Spread Spectrum Multiple Access Communication-Part I: System Analysis," *IEEE Transactions on Communications*, vol. COM-25, pp. 795–799, August 1977.

[40] Q. Shi and M. Latva-aho, "Effect of Frequency Offset on the Performance of Asynchronous MC-CDMA Systems in a Correlated Rayleigh Fading Channel," in *IEEE International Conference on Info-tech and Info-net*, vol. 2, pp. 448–452, October 2001.

[41] J. G. Proakis, *Digital Communications.* McGraw Hill,New York, fourth ed., 2001.

[42] X. Qiu and K. Chawla, "On the Performance of Adaptive Modulation in Cellular Systems," *IEEE Transactions on Communications*, vol. 47, pp. 884–895, June 1999.

[43] W. T.Webb and R. Steele, "Variable Rate QAM for Mobile Radio," *IEEE Transactions on Communications*, vol. 43, pp. 2223–2230, July 1995.

[44] K. Chang and Y. Han, "OFCDM based Adaptive Modulation with Antenna Array in Fading Channels," in *IEEE Vehicular Technology Conference*, vol. 1, pp. 122–126, April 2003.

[45] J. Torrence and L. Hanzo, "Upper Bound Performance of Adaptive Modulation in a Slow Rayleigh Fading Channel," *IEEE Electronics Letters*, vol. 32, p. 718, April 1996.

[46] X. Duan, X. Ma, Z. Niu, and J. Zheng, "Analysis of Wireless Transmission Efficiency and Its Application: Efficiency-Based Adaptive Coding," in *IEEE International Symposium on Personal, Indoor and Mobile Radio Communications*, vol. 2, pp. 1516 – 1520, September 2003.